

## Article

# Assessment of the Impact of Emitted Radiated Interference Generated by a Selected Rail Traction Unit on the Operating Process of Trackside Video Monitoring Systems

Jacek Paś <sup>1</sup>, Adam Rosiński <sup>1,\*</sup>, Patryk Wetoszka <sup>2</sup>, Kamil Białek <sup>2</sup>, Tomasz Klimczak <sup>3</sup> and Mirosław Siergiejczyk <sup>4</sup>

<sup>1</sup> Division of Electronic Systems Exploitations, Institute of Electronic Systems, Faculty of Electronics, Military University of Technology, 2 Gen. S. Kaliski St., 00-908 Warsaw, Poland

<sup>2</sup> Signalling and Telecommunications Laboratory, Railway Research Institute, 50 Chłopickiego St., 04-275 Warsaw, Poland

<sup>3</sup> Constructions Safety Department, The Main School of Fire Service, 52/54 J. Słowackiego St., 01-629 Warsaw, Poland

<sup>4</sup> Division Telecommunications in Transport, Faculty of Transport, Warsaw University of Technology, 75 Koszykowa St., 00-662 Warsaw, Poland

\* Correspondence: adam.rosinski@wat.edu.pl



**Citation:** Paś, J.; Rosiński, A.; Wetoszka, P.; Białek, K.; Klimczak, T.; Siergiejczyk, M. Assessment of the Impact of Emitted Radiated Interference Generated by a Selected Rail Traction Unit on the Operating Process of Trackside Video Monitoring Systems. *Electronics* **2022**, *11*, 2554. <https://doi.org/10.3390/electronics11162554>

Academic Editors: S. M. Muyeen, Jahangir Hossain, Mohamed Benbouzid, Antonio J. Marques Cardoso and Marco Mussetta

Received: 22 June 2022

Accepted: 11 August 2022

Published: 15 August 2022

**Publisher's Note:** MDPI stays neutral with regard to jurisdictional claims in published maps and institutional affiliations.



**Copyright:** © 2022 by the authors. Licensee MDPI, Basel, Switzerland. This article is an open access article distributed under the terms and conditions of the Creative Commons Attribution (CC BY) license (<https://creativecommons.org/licenses/by/4.0/>).

**Abstract:** The article presents a method for assessing the impact of radiated electromagnetic interference generated by a selected rail traction unit on the operational process of trackside video monitoring systems (VMS). VMSs operated throughout an extensive railway area are responsible for the safety of people and property transport processes. Emissions of radiated electromagnetic interference generated in an unintended manner by traction vehicles within a railway line lead to interference in the VMS operating process. Based on the knowledge of actual VMS operating process data, spectral characteristics and values of individual components of disturbing signals occurring in the emissions of radiated electromagnetic interference, it is possible to determine the parameters of damage intensities for the devices and elements of this system. Using that data enables determining the VMS reliability parameters within its operating system, for an extensive railway area. The article's authors first discussed the basic issues associated with VMS, followed by analysing the topic's current status. They also presented issues related to measuring interference radiated within a rail area, developed a selected operational process model, and determined selected operational indicators for the structures in question. The paper ends with conclusions.

**Keywords:** video monitoring system (VMS); radiated electromagnetic interference; damage intensity; system model; reliability

## 1. Introduction

Video monitoring systems (VMSs) are one of the most important electronic security systems (ESS). They operate in buildings, open areas, parking lots, logistics bases, airports, etc., and extensive public and railway areas [1–3]. Depending on the operational mode within extensive areas in warehouse and railway facilities, VMSs can be divided into two groups:

- Stationary, i.e., operated in facilities permanently set on the ground (foundations), e.g., railway stations, platforms, tunnels, level crossings, turnpikes, underground passages, warehouses and logistics bases storing spare parts, repair workshops, parking spaces—parking lots, warehouse buildings, driveways, etc. [4–6];
- Non-stationary (facilities not permanently fixed to the ground)—e.g., locomotives, electric multiple units, electric locomotives, passenger and freight carriages, trucks, mass transit vehicles and vehicles intended for transporting various materials, etc. [7–9].

Both VMS and all ESSs (especially the fire alarm system—FAS) must send information on their ongoing technical status via two independent telecommunication channels to an Alarm Receiving Centre (ARC) or the State Fire Service (PSP) [10]. The most important ESS operational technical states include the states of alerting, monitoring and damage, whereas the latter is sent only to ARC in the case of FAS [11]. The use of two independent telecommunications channels to exchange information within security systems is associated with ensuring a certain level of reliability, especially in the case of alerting states [12]. In the case of stationary and non-stationary VMSs within a railway area, the facilities of which are classified as the so-called state critical infrastructure (SCI), it is essential to ensure proper organization of the entire system notifying of threats within a railway area and not only the VMSs [12,13]. This is why the following telecommunications lines are set up for stationary and non-stationary VMSs:

- Stationary VMS—Permanent telecommunications link in the form of a leased telephone line using a railway optical fibre network (protected against wide-frequency band electromagnetic interference within the railway area), as well as a wireless (encrypted) link with a modular signal, which is IT-protected against an intentional third-party and internal attack [14,15];
- Non-stationary VMS—Two independent wireless telecommunications links utilizing various transmitter carrier frequencies, modulated with a digital signal in alarm control units (ACU), which are resistant to electromagnetic interference generated within an extensive railway area, encrypted with appropriate transceiving antenna characteristics [16,17].

In addition, in the case of stationary and non-stationary VMSs, all technical facilities that utilize this system shall be equipped with a local device for recording video-recorder signals of specified external memory size, the technical parameters of which are set out in domestic regulations (e.g., stadiums) [18–20].

A supplementary and very important issue associated with the VMS and ESS operation process is ensuring specific power supply reliability for these systems operated in a stationary and non-stationary manner [21,22]. ESS shall have ensured basic power supply—from an industrial power grid (stationary facilities) or via transducers from a railway overhead contact line (3 kV DC) (non-stationary facilities) [23,24]. Backup power supply, most often in the form of a battery bank of specific capacity determined by the power balance, is organized in order to guarantee proper ESS functioning in the event of basic power supply failure. This guarantees the functioning of these systems in the monitoring and alerting modes for a time specified by regulations and standards [25,26]. Information on the technical condition of a backup power supply (e.g., battery bank or UPS voltage level, etc.) shall be monitored continuously by the security system alarm control unit, and the information regarding this parameter should be sent to ARC, just like other security signals. In addition, battery banks are located in a metal housing with ACU. The metal housing is locked with a coded lock. In addition, it is monitored with an anti-tampering contact, which generates an alert signal in the event of an unauthorized opening [12,25].

An extensive railway area experiences a distorted electromagnetic environment generated by stationary (radio transmitters and TV transmitters, GSM-R, power supply and overhead contact network, etc.) or non-stationary (electric multiple units, rail carriages, portable security system transmitters, etc.) radiation sources [27,28]. Electromagnetic radiation within a railway area is generated intentionally—e.g., wireless signals of security systems, cellular telephony such as GSM—these signals will be used by authorized railway services. Other sources generate unintentional electromagnetic radiation—e.g., power supply, railway overhead traction lines, high current and voltage consumers—e.g., traction converters, locomotive motors present within these areas [29,30]. Electromagnetic interference generated within a railway area is characterized by a very broad spectrum, from low (single Hz) to very high (single GHz) frequencies. This is due to this railway system accumulating various sources of radiation used by railway workers, as well as

power supply and overhead contact line systems used by the pantographs of electric locomotives to draw high-value current (in the order of several dozen kA) upon startup for a short period. It is a serious problem related to the distortion of the electromagnetic environment within such a railway area. Therefore, conducted and radiated interference shall be considered [31–33]. The selected aforementioned issues of ESS and VMS operation throughout an extensive railway area are presented in Figure 1.

Figure 1 shows only the selected operational aspects of ESS use within an extensive railway area. The geometric figure in No. 12 shows examples of regions with low and high-frequency band electromagnetic interference originating only from overhead contact lines and systems supplying the entire railway area. High-frequency band electromagnetic interference, so-called radiated interference, occurs throughout the railway area, and its value depends on, among others, distance from the source of a signal generated intentionally or unintentionally.

The rest of this article is organized as follows. Section 2 is a critical review of the source literature on the current state of the issue in question. The analysis of fundamental issues related to the measurement method and test results involving interfering electromagnetic signals make up Section 3. Section 4 presents a reliability and operation simulation of a CCTV system for selected damage intensities. It also contains simulation results. The final, fifth chapter contains conclusions arising from the conducted tests and computer simulations.

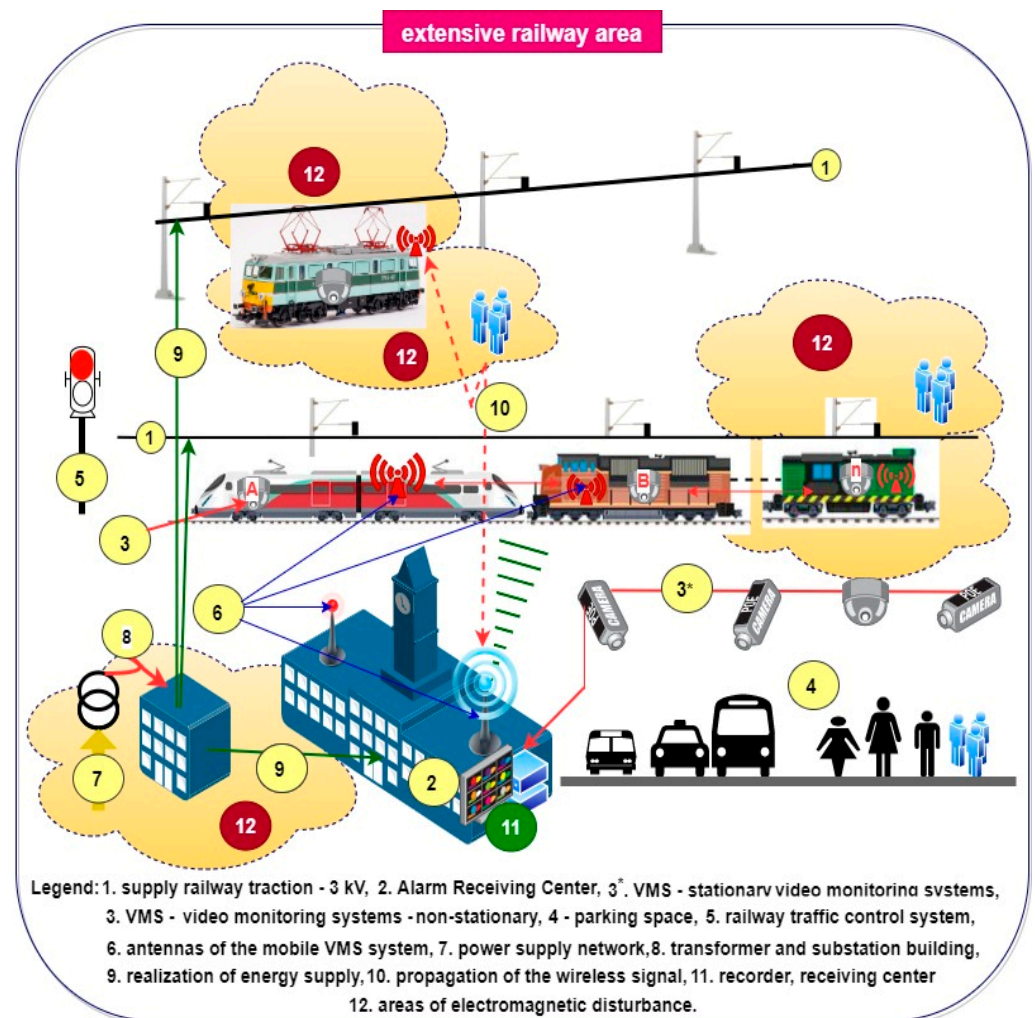


**Figure 1.** Operational issues, i.e., environment, electromagnetic interference, legal restrictions, telecommunications, etc., resulting from VMS within a railway area.

## 2. Literature Review

Variable environmental conditions, a change in low- and high-frequency electromagnetic interference level in particular (conducted, coupled L, C and radiated interference) is one of the significant factors [34–36] leading to a direct change in the damage intensity  $\lambda$ . This operating parameter  $\lambda$  directly impacts the reliability of VMS elements, modules and devices, as well as VMS functioning. Therefore, the authors of [37–39] discussed electromagnetic interference from the entire frequency band generated within an extensive railway area, specifying their levels, amplitudes and spectra [40,41]; however, they failed to analyse their impact on the reliability of individual system elements (e.g., camera, recorded, switch, etc.) or the entire VMS.

Variable, pulsed, and non-linear power supply line loads of high inrush currents can present within an overhead railway line and lead to current harmonics appearing in power supply lines [42–44]. They can cause VMS and ESS functioning interference and be the reason for additional losses in transformer cores and traction vehicle startup motors. The pulsed loads occurring within the power supply and overhead contact networks also cause changed rated voltages [45,46]. This may lead to unacceptable changes in the guaranteed voltage level ( $U = 12\text{ V}$ ) for individual VMS elements [43,47]. The presence of harmonics in a power supply and overhead contact network [48,49] also means additional losses in the cables themselves, especially the ones supplying individual VMS and ESS elements (e.g., cameras), which are distributed throughout an extensive railway area (e.g., failure to satisfy the condition of permissible supply line voltage dip) [50–52]. The presented source literature on the phenomena in power supply lines does not reference a change in damage intensity  $\lambda$ . The studies conducted by the article's authors enable assessing the impact of the aforementioned interference on VMS reliability.

A variable, pulsed load in an overhead contact line and power lines supplying an extensive railway area cause electromagnetic interference of large amplitudes from within the entire frequency band [53–55]. The occurring electromagnetic interference that causes conducted interference (e.g., common grounding impedance), inductance coupling or parasitic capacitances for VMS elements or devices through signal lines or cables providing the supply voltage [56–58]. Conducted interference from a higher frequency band (above 30 MHz) propagates into the surrounding space within a railway area through the generally available environment [59,60]. Individual VMS elements and devices with external conduits or metal housings with openings and wide bandwidth antennas are treated by these interfering signals as parasitic signal receivers [61]. In their articles, the authors did not analyse the impact of interference on the reliability of electronic components. In the case of non-linear elements that comprise VMS, these signals may interfere with or change the processing characteristics or cause the presence of intermodulation phenomena [62,63]. In the course of studying the characteristics of radiated interference generated within a railway area, a method was proposed that would enable the determination of a change in the intensity index  $\lambda$  for VMS elements or equipment operated within such a railway area.

An important issue related to security systems, including VMS, is also the process of diagnosing their technical condition [64–66]. Generally available articles and studies present general assumptions of measurement systems that implement this important operational process under the following static and dynamic conditions, employing various diagnostic techniques and technical solutions [12,17,67]. However, these studies do not take into account the impact of natural or artificial electromagnetic interference present within a railway area. They result from, e.g., long signal loops of cameras, control lines for PTZ cameras and devices transmitting an alert or damage state [17,68,69]. The authors of the said papers mitigated these errors contributed by interfering signals [12,70]. Testing the electromagnetic interference present in a railway environment, as well as the observation and measurement of output signals in alarm control units where the decision-making process takes place—i.e., conditioning and working out output waveforms—enables determining the impact of the aforementioned factors, e.g., on the output signal informing about the monitoring, alerting or damage state, or other forced operation process [12,17,65,71].

An important issue associated with the VMS operation processes is the transmission of video, alerting, monitoring, or damage signals to ARC [12,72,73]. The authors of published articles took only the basic problems into account. This included reliability, availability, quality or, e.g., transmission time to ARC [17,74,75]. In contrast, the authors of the developed article also conducted an analysis of notification and ARC service response to a damage signal [12,17,76]. The calculations conducted as part of this article included this parameter, e.g., in VMS recovery intensity  $\mu$  [12,17,77]. It is an issue that is particularly important for restoring a VMS to an original (initial) state—i.e., the state of fitness of an entire system [78–81].

The authors were unable to find cases (research, results, as well as theoretical analysis) focusing on the impact of unintentional electromagnetic field emissions within this frequency range on the operation process of electronic systems, VMS in this case, within the analysed articles presented in the critical source literature review. A railway VMS system is responsible for traffic safety. It is one of the priority systems besides the railway traffic control system. The article is the first of its kind in this field, which addresses issues associated with the impact of unintentional electromagnetic field emissions within a selected frequency range on the operation process, i.e., reliability or the availability factor. This is preliminary research, and the authors plan to extend it to various rail vehicles.

### 3. Analysis of Basic Issues Related to the Method of Measuring Radiated Interfering Electromagnetic Signals and Test Results

The intensities of radiated electromagnetic fields generated over an extensive railway area were measured in accordance with applicable legal regulations, namely the PN-EN 50121 series of standards applicable in Poland and the European Union. The tests were conducted within the premises of the Railway Institute Test Track Operation Centre (OETD) for cases of an electric locomotive travelling at a specific speed, over a railway track, and in a static, i.e., parking, state, in accordance with the PN-EN 50121-3-1 and PN-EN 50121-2 standards. Satisfying specific technical requirements is important in order to conduct the tests (position of the measuring point at the OETD).

Determining the magnitude of low-frequency and radiated electromagnetic interference occurring within a vast railway area requires identifying the following technical parameters exhibited by power supply circuits:

- So-called high-current power supply circuits, i.e., traction substations, overhead contact line, traction vehicle consumer network;
- So-called low-current power supply circuits, e.g., rail traffic control systems, telecommunications systems, electronic security systems—including VMS surveillance TV, etc.

Electromagnetic interference generated by a substation and traction vehicles is asynchronous due to the DC railway overhead traction line, unlike AC overhead contact lines, which experience synchronous interference, as shown in Figure 2. An AC traction has a one-sided power supply, which means that each next railway overhead contact line is powered from a different phase. The interference (interference spectrum) generated within an overhead contact line and by traction vehicles are synchronized with the fundamental frequency for a given traction power supply system.

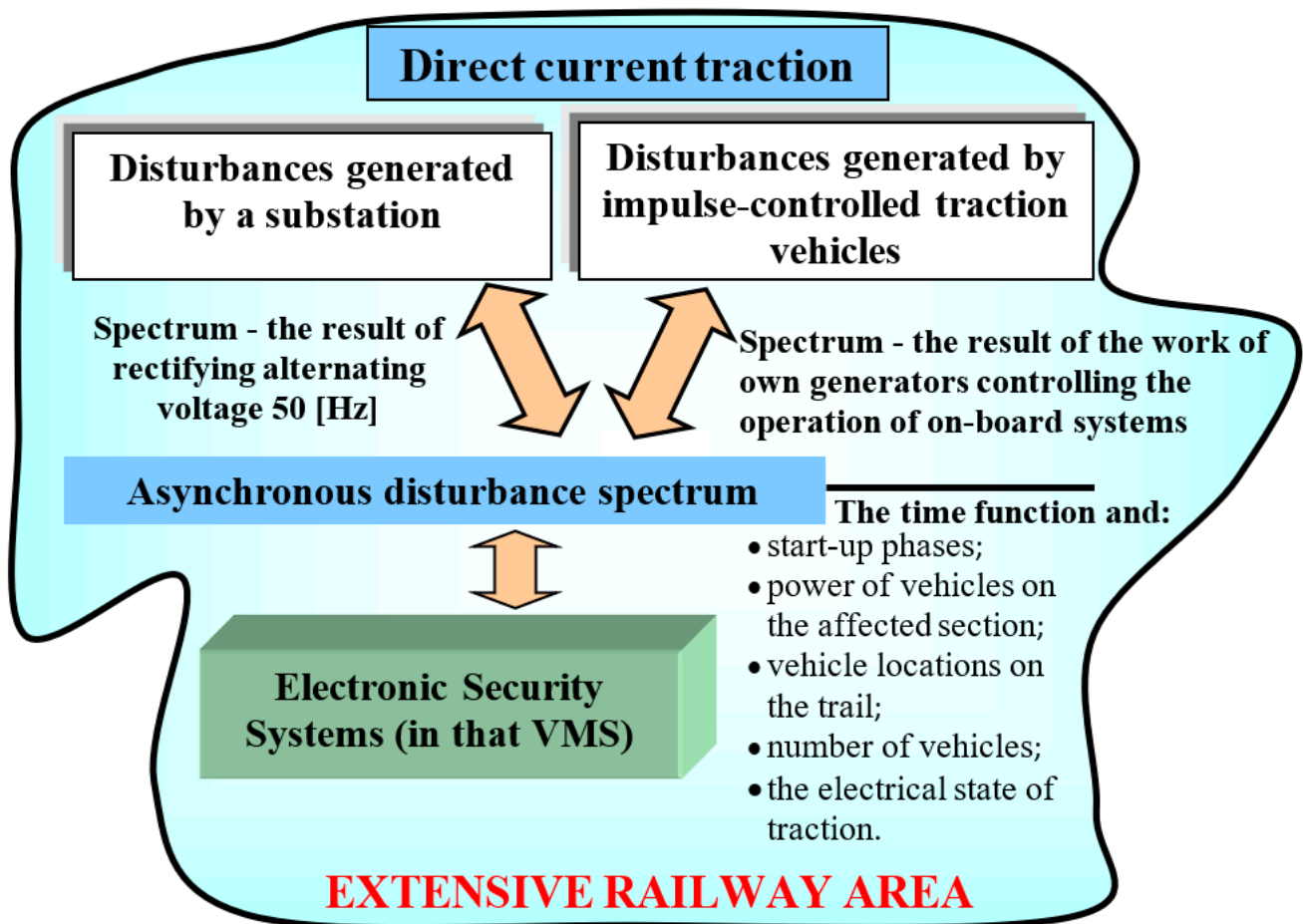


**Figure 2.** Electromagnetic interference generated by a power substation and traction vehicles over a vast railway area and its impact on VMS.

Within an overhead contact line supplying railway vehicles, the value and shape of the interfering variable component and the radiated electromagnetic field emissions are impacted by the following parameters:

- Values of currents generated by individual consumer sources  $Z_{X1} = f(t)$ ,  $Z_{X2} = f(t)$ ,  $\dots$ ,  $Z_{Xn} = f(t)$ —impedances for individual traction vehicles within a railway line;
- Interfering variable components generated by overhead contact line power supply substations  $Z_1 = f(t)$ ,  $Z_2 = f(t)$  under the influence of a variable load and having its own load signal processing characteristics  $I_1(t)$ ,  $I_2(t)$ ,  $\dots$ ,  $I_n(t)$ .

The value of radiated interference occurring within an overhead contact line is also impacted by the current location of a given traction vehicle within the line and its impedance relative to this point. Individual radiated emission interfering signals generated by current consumers (traction vehicles) also depend on the amplitudes and phases of harmonics originating from individual traction substations  $Z_1 = f(t)$ ,  $Z_2 = f(t)$ , as shown in Figure 3.

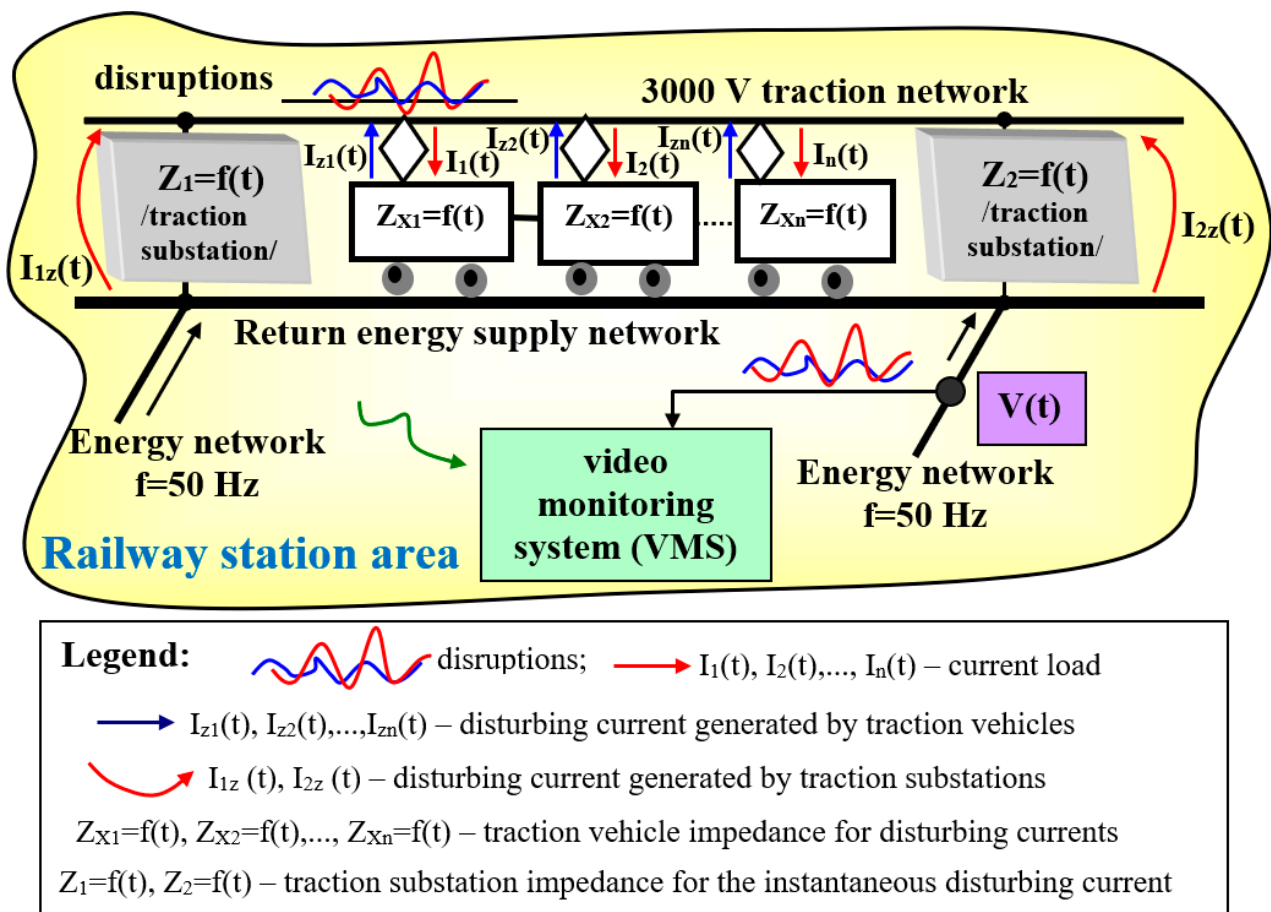


**Figure 3.** Generating low-frequency interference and EMI radiated signals by current consumers (traction vehicles) and overhead contact line power supply substations over a vast railway area.

The most important issues related to the position of the measurement stand and the lack of external environmental impact [82–85] on measurement accuracy include:

- No large vegetation, shrubs, and trees in the nearest vicinity (approximately 30 m) around the measuring point, which would significantly distort the electric field for different frequency bands;
- No railway buildings, metal fences, traction substations or power grid transformer stations would adversely impact the electromagnetic environment throughout the entire frequency range, as shown in Figure 4;
- No other systems, e.g., railway traffic control systems, blocks, or line control systems (LCS);
- No other traction vehicles in the vicinity of a measurement point, moving along the same tracks or in a state of parking, which may or may not be powered from an overhead contact line. Rail vehicles may be the source of secondary electromagnetic radiation (wave reflection, interference, etc.) or may spontaneously and unintentionally generate their own electromagnetic field that will impact the accuracy of conducted measurements.

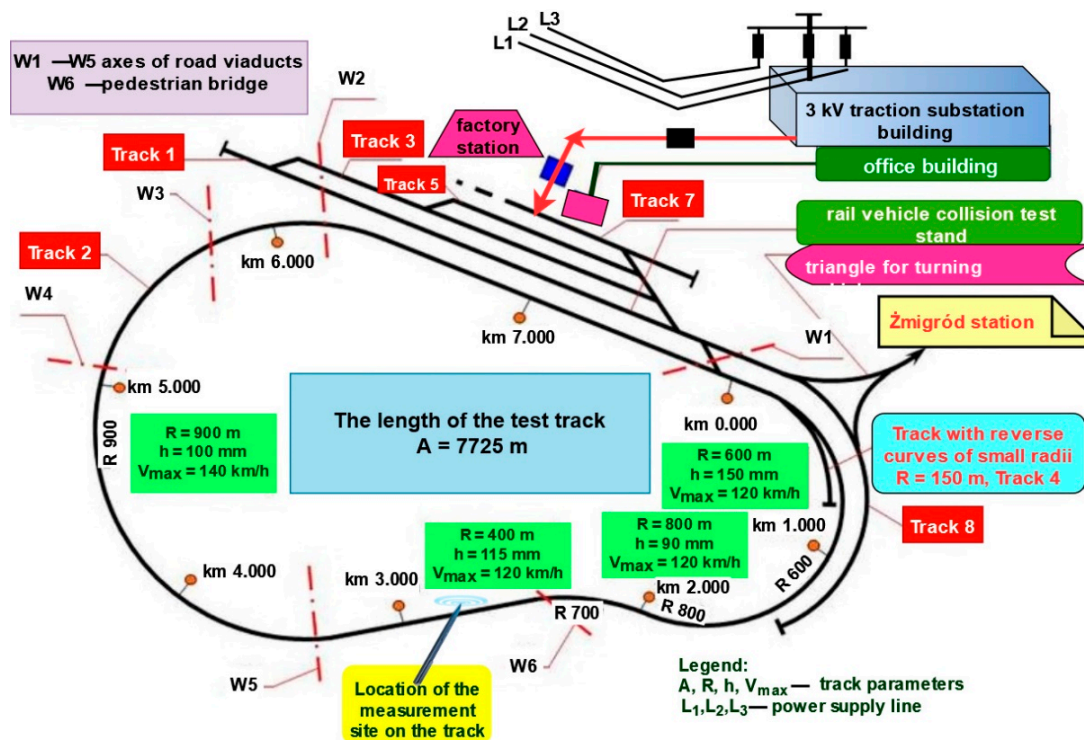


**Figure 4.** The Railway Institute's test track located near Żmigród. The measurement point of radiated interfering signals is marked in the figure.

The electromagnetic compatibility tests discussed in the article were conducted at the Railway Institute Test Track located near Żmigród, as shown in Figure 4. It is a curvilinear, closed, circular and 7725 m long track. It has a straight section of more than 1 km, which enables testing the dynamic behaviour of rail vehicles, with a rail track speed limit equal to 160 km/h, as shown in Figure 4.

Approving a rail vehicle to traffic on a railway route, in accordance with legal regulations applicable in Poland, requires, among others, measuring the emission of radiated interference. It is one of the frequency ranges of unintentional electromagnetic radiation generated by a rail vehicle travelling on a track. It is associated with the high electricity consumption by the pantograph from an overhead line (3 kV DC) and the processing of signals in drive systems (devices)—traction converters and motors [86–89]. Electromagnetic compatibility (EMC) tests not only involve radiated interference frequency but also require measuring the magnetic and electric field within the low-frequency ranges—up to 100 kHz. This article refers to the impact of higher frequency ranges on one of the security systems installed and commonly operated within a railway area, namely, a CCTV system. When considering the impact of the electromagnetic field from the entire spectrum of interfering signals on electronic elements and devices, individual frequency subranges should be taken into account separately [10,90]. These ranges should be divided in accordance with the current division applicable to the method for measuring electromagnetic compatibility. Electromagnetic interference penetrates electronic elements and devices of ESS in various ways, e.g., mutual low-frequency range impedance, parasitic inductances or PCB capacitances or the phenomenon of interfering electromagnetic field radiation. In this case, a travelling railway vehicle is a common source of undesired signals. One of the many electromagnetic compatibility tests required by appropriate authorities (e.g., Office of Rail Transport) to approve a vehicle to operate within the Polish railway infrastructure is the test involving radiated interfering electromagnetic signals. The test should be conducted in accordance with the methodology set out in PN-EN 50121-3-1 and PN-EN 50121-2, within

a strictly defined frequency band, from 150 kHz to 1 GHz, using specialized measuring antennas that take into account the division into two measurement subranges:

- Measurement of the magnetic component of electromagnetic field strength in the frequency range: 150 kHz ÷ 30 MHz using a frame (loop) antenna;
- Measurement of the electric component of electromagnetic field strength in the frequency range: 30 MHz ÷ 1 GHz using two antennas: biconical and log-periodic.
- Whereas the traction unit itself is tested in two operating modes:
- During parking (stationary), with all power consumers onboard the rail vehicle switched on and consuming maximum power;
- During travel (dynamic) with the permissible speed equal to  $50 \pm 10$  km/h.

During the measurement of the electromagnetic compatibility for the two-rail vehicle operating modes referred to above, all devices and systems installed onboard the vehicle, i.e., A/C system, ETCS, passenger information system, internal and external lighting, including electronic security systems installed within such a technical structure are switched on. The traction vehicle should then be consuming maximum power (current) from the 3 kV supply overhead line. In the event of in-parking tests, the measurement point is set where the highest level of the vehicle's radiated interference is emitted. It is determined using trial runs and a measuring antenna. Measurement during parking is conducted using a quasi-peak detector. Whereas in the travel mode, the traction vehicle should accelerate or decelerate, using 1/3 of the maximum tractive force, within a strictly defined speed range. In order to eliminate interference originating from the 3 kV overhead line current collector, the in-test speed was limited to 50 km/h and the power to 1/3 of the maximum tractive force.

The basic and main device (measurement sensor) used when measuring electromagnetic compatibility are appropriate antennas, positioned at a specific distance (10 m) from the track axis, at different heights above the ground, depending on the type of the employed antenna:

- Loop—1 m ÷ 2 m above the railway line rail head, as shown in Figure 5;
- Biconical and log-periodic—2.5 m ÷ 3.5 m above the railway track head, as shown in Figures 6 and 7, respectively.

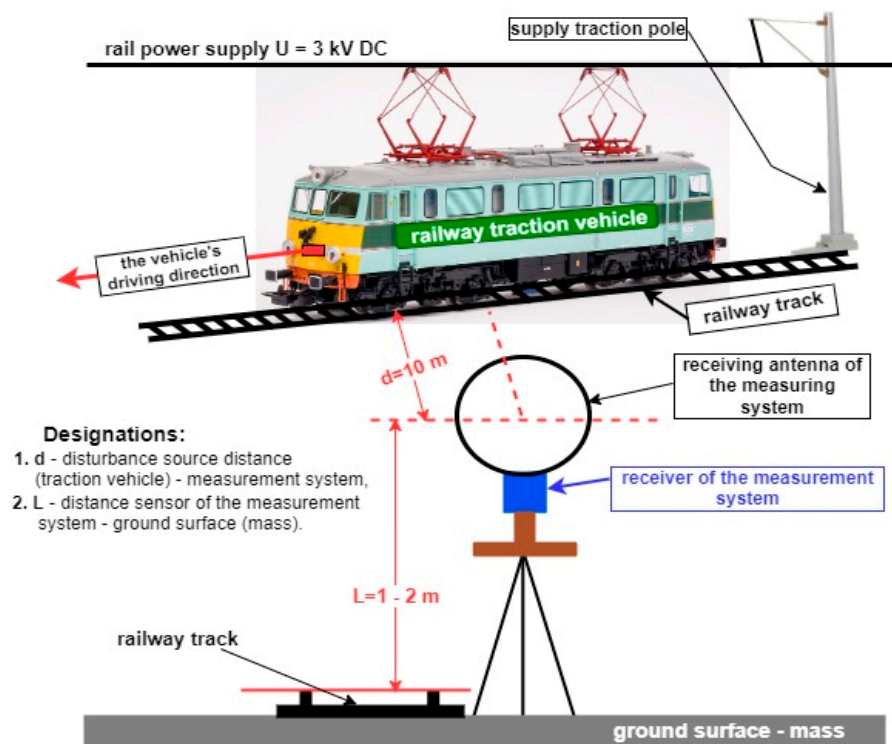


**Figure 5.** Measurement of radiated interference emission in the 150 kHz ÷ 30 MHz frequency band using a loop antenna.

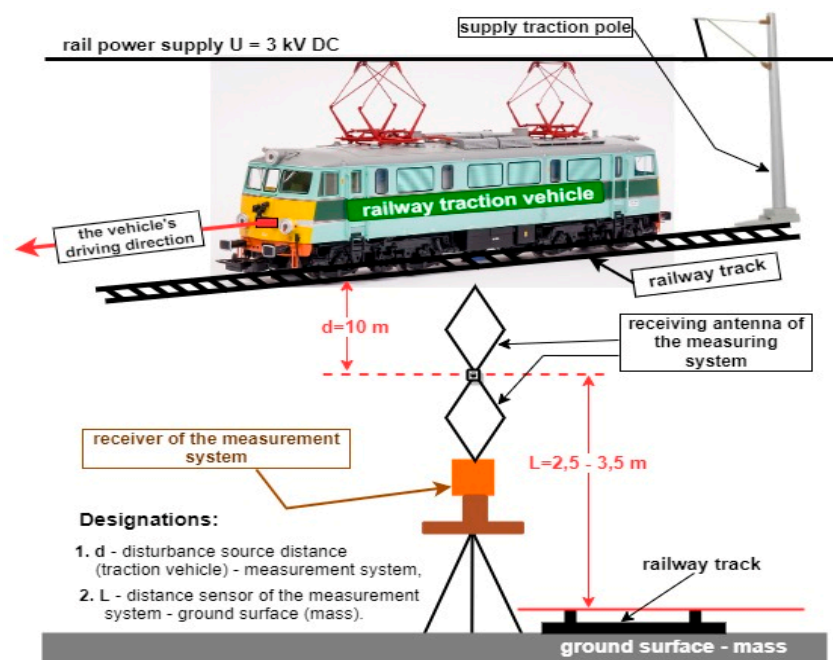


Figure 6. Measurement of radiated interference emission in the 30 kHz ÷ 230 MHz frequency band using a biconical antenna.

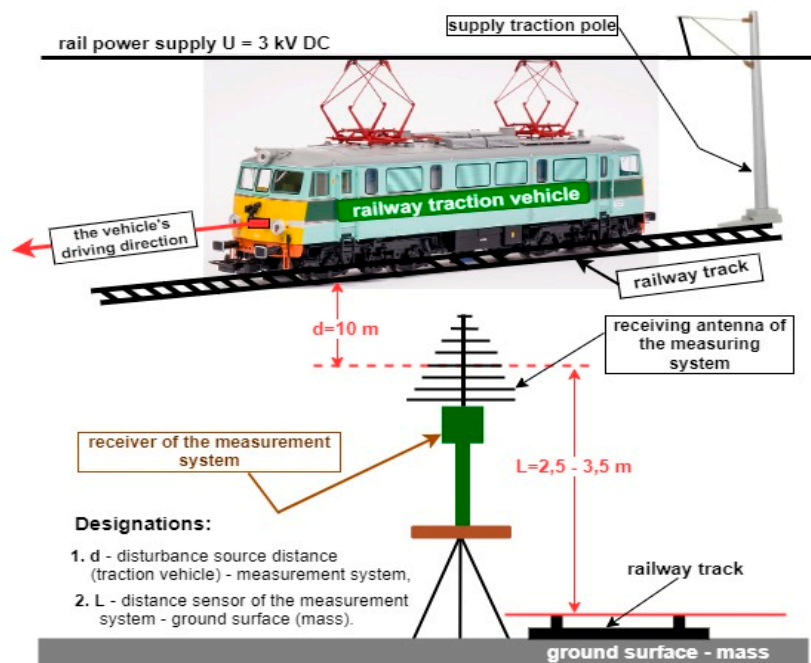


Figure 7. Measurement of radiated interference emission in the 230 MHz ÷ 1 GHz frequency band using a log-periodic antenna.

The antenna suspension height during the measurements is selected to ensure the readings of the maximum level of electromagnetic field interference, which are emitted by a rail vehicle. The measurement shall be conducted in accordance with the applicable PN-EN 50121-3-1 standard for two antenna polarizations (V—vertical and H—horizontal). The stands for measuring electromagnetic compatibility within this frequency range have been appropriately illustrated in Figures 5–7, using different types of measuring antennas. The figures also contain the permissible antenna heights above the ground, the measurement

distance from the rail vehicle and the method of antenna distribution relative to the rail vehicle—moving or parking.

Electromagnetic compatibility was measured for radiated interference in the two distinguished rail vehicle operating modes using various antennas intended to measure over strictly defined frequency ranges. The antennas are also positioned at specific distances, defined in the standard covering the methodologies of testing a distorted electromagnetic environment around a rail vehicle. The list of employed antennas and their frequency subranges, as well as measurement distances, suspension heights and position, have been shown in Table 1.

**Table 1.** Basic technical parameters of measuring antennas. Suspension height, distance, and position relative to the interfering object (source).

Antenna Type	Frequency Band	Measurement Distance	Antenna Suspension Height	Antenna Positioning
FMZB 1513	150 kHz–30 MHz	10 m	1.5 m	Parallel to track axis
VBA 6106A	30 MHz–230 MHz	10 m	3 m	Vertical (V) and horizontal (H)
VUSLP 9111B	230 MHz–1 GHz	10 m	3 m	polarization

Figure 8 contains photographs—of the appearance of actual measurement stands located within the Railway Institute Test Track. On the other hand, Figure 4 marks the location of electromagnetic compatibility tests within the range of radiated interfering signals. The measurement point satisfies the requirements set out in the standard covering the measurement methodology. Failure to meet this requirement means unintentional changes to the original electromagnetic field “signature”.

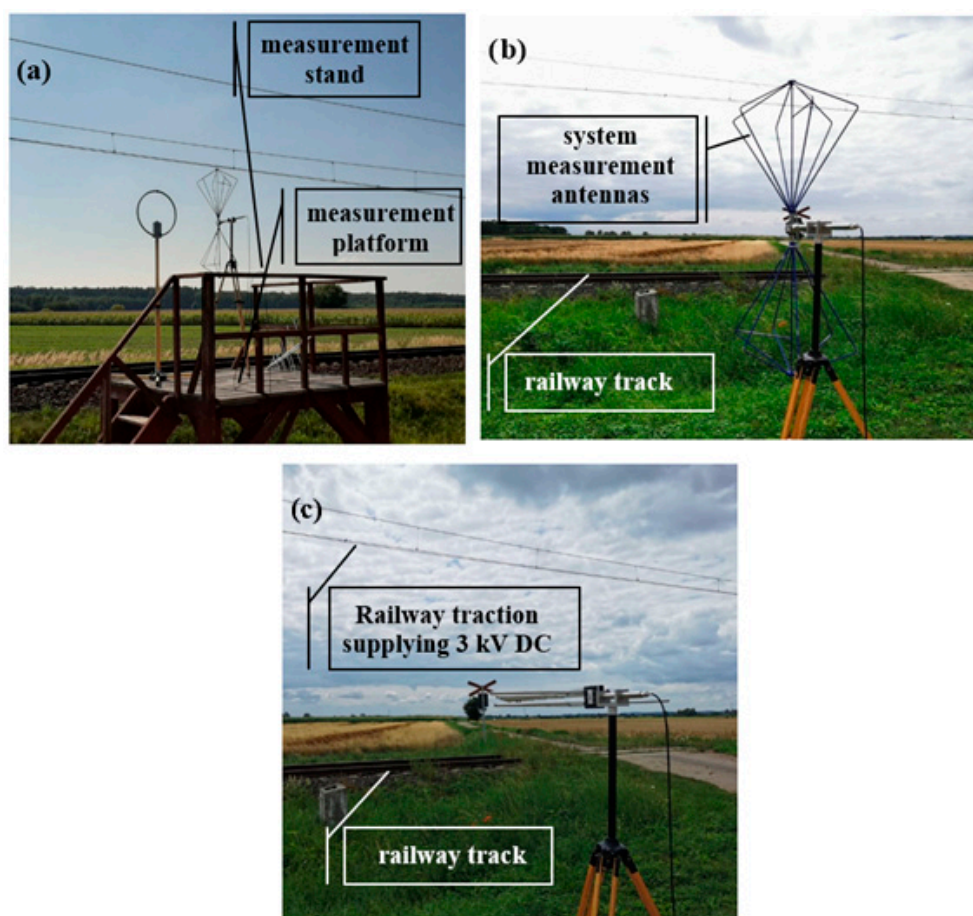


**Figure 8.** Appearance of actual measurement stands located within the Railway Institute Test Track for various types of measuring antennas.

During the entire measuring process (2 working days), the measurements were conducted with a positive ambient temperature of +14 °C, with no precipitation and fog. Air relative humidity during the days of the measurements amounted to 59%. Environmental conditions greatly affect measurement credibility, which is why the measurements are taken under specific conditions, e.g., ambient temperature of at least +5 °C. Such measurements are conducted primarily in the spring-autumn period, where the temperature and humidity values fall within the standard range.

A modern rail vehicle, which is currently being introduced to the Polish transport market, was chosen for measuring electromagnetic field emissions. The rail vehicle is fitted with state-of-the-art technical solutions in onboard electronic systems and the drive itself (traction motors, converters, data transmission network, passenger information system, onboard railway traffic control systems, ETCS, etc.). Obsolete traction units with electromechanical controls are currently being withdrawn and replaced with electronically controlled locomotives with power-electronic systems and in hybrid technology.

### *3.1. Results of Electromagnetic Compatibility Tests within the Frequency Range of Radiated Interfering Signals*

The radiated emission measurements within the frequency range of 150 kHz to 1 GHz involved 10 electromagnetic field measurements. The authors of this article provided a mean electromagnetic field value for  $n = 10$  for this frequency range. Individual spectral line amplitudes of unintentional electromagnetic field signals measured for this frequency range indicate a maximum deviation from the mean values in the graphs of  $\pm 10\%$ . Electromagnetic field emissions were repeatable since the research paper's authors conducted them on a straight-line test track section (rail vehicle did neither accelerate nor decelerate). The rail vehicle was constantly moving and had all electrical current consumers required for correct functioning pre-activated at the parking station.

Figures 9–14 show interfering signal spectra for different frequency ranges obtained during the measurements. These figures illustrate two different spectrum waveforms within the discussed frequency subranges and permissible values for a given frequency range, as set out in the PN-EN 50121-3-1 standard. Figure 9 illustrates the spectrum of interfering signals radiated by a rail vehicle travelling at 50 km/h for a frequency range of 150 kHz–1.15 MHz. The waveform values obtained during the measurement are shown in all Figures using different waveform colours and appropriately marked using the letters A, B and C:

- A—Permissible values for a given frequency range, set out in the PN-EN 50121-3-1 standard;
- B—Electromagnetic field values obtained during the measurements for a rail vehicle travelling along the OETD at a speed of 50 km/h;
- C—Electromagnetic field values were obtained during the measurements of the electromagnetic background at the OETD.

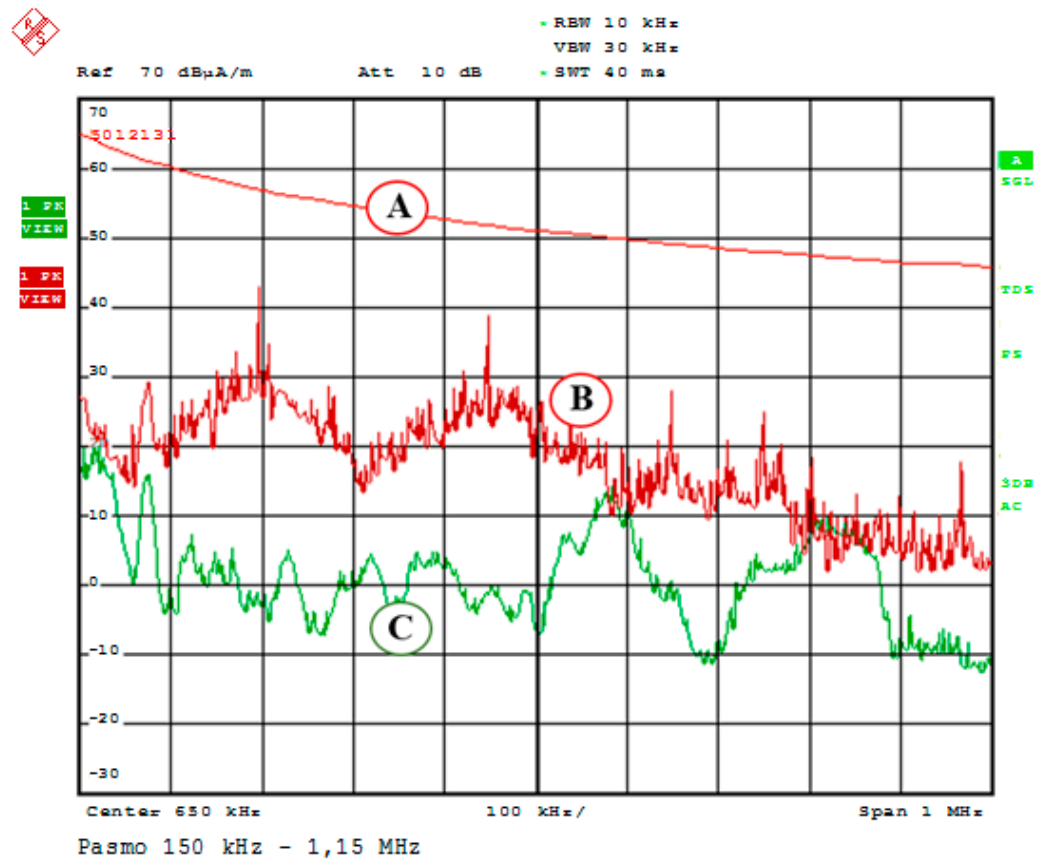


Figure 9. Spectrum of interfering signals radiated by a rail vehicle travelling at a speed of 50 km/h and the electromagnetic background for a frequency range of 150 kHz–1.15 MHz.

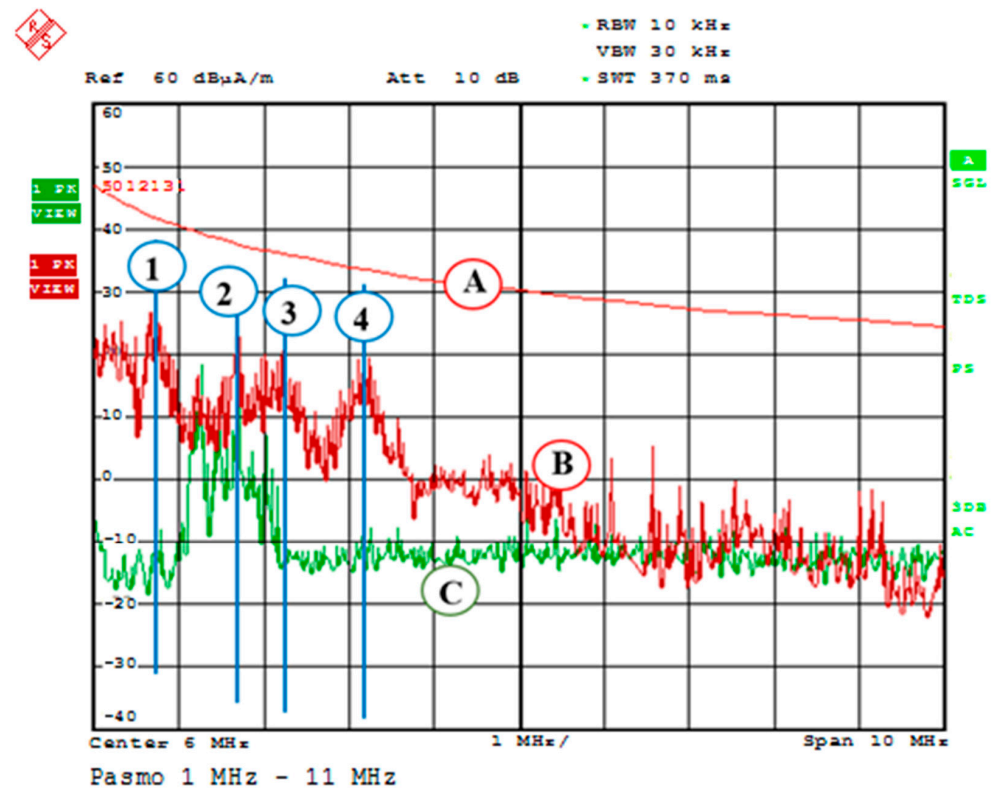


Figure 10. Spectrum of interfering signals radiated by a rail vehicle travelling at a speed of 50 km/h and the electromagnetic background for a frequency range of 1 MHz–11 MHz.

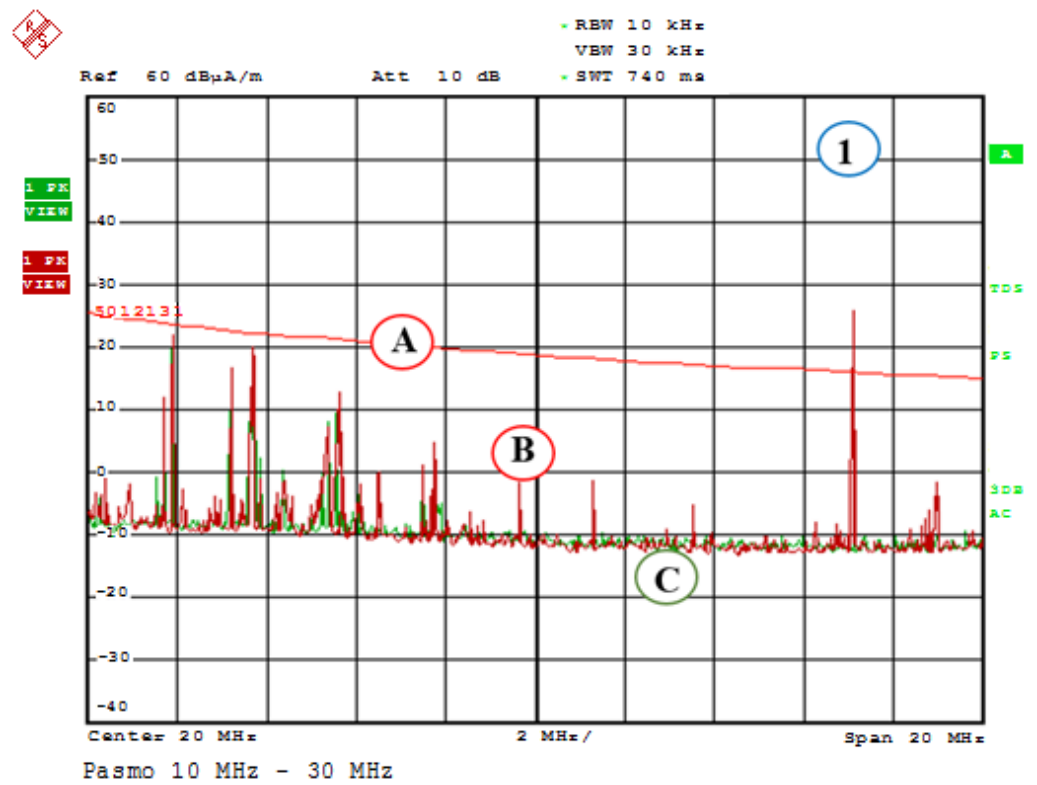


Figure 11. Spectrum of interfering signals radiated by a rail vehicle travelling at a speed of 50 km/h and the electromagnetic background for a frequency range of 10 MHz–30 MHz.

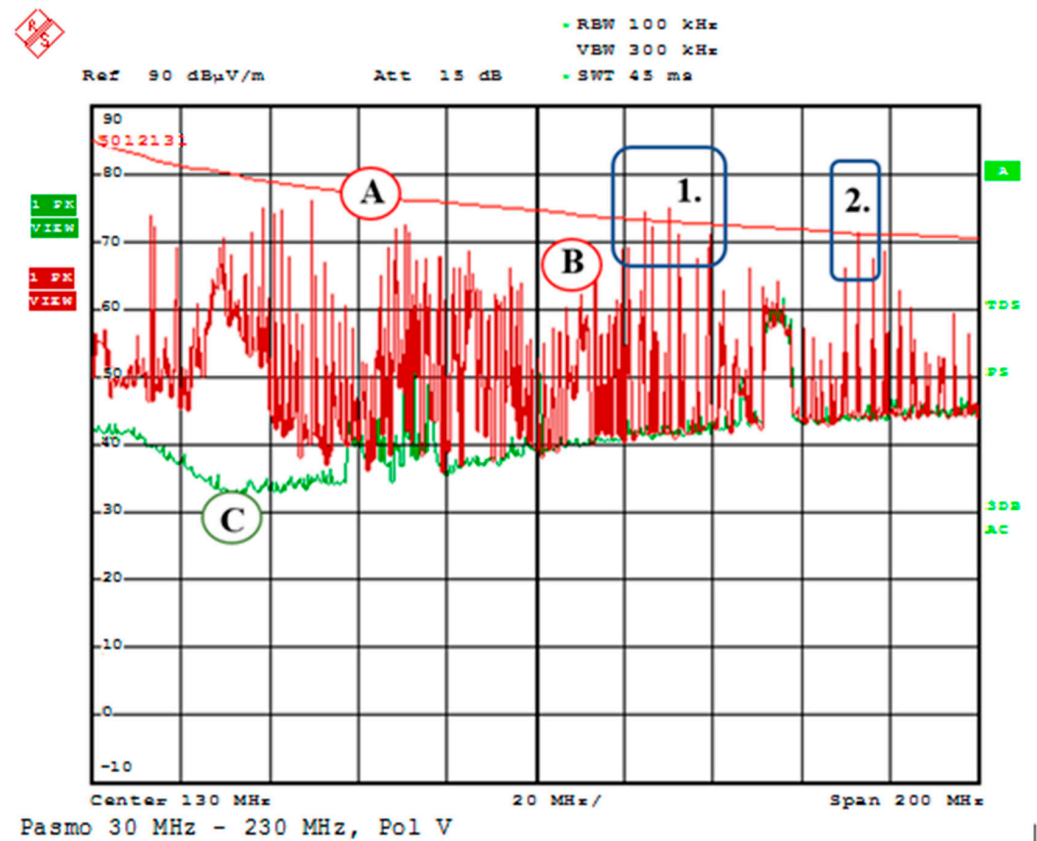


Figure 12. Spectrum of interfering signals radiated by a rail vehicle travelling at a speed of 50 km/h and the electromagnetic background for a frequency range of 30 MHz–230 MHz.

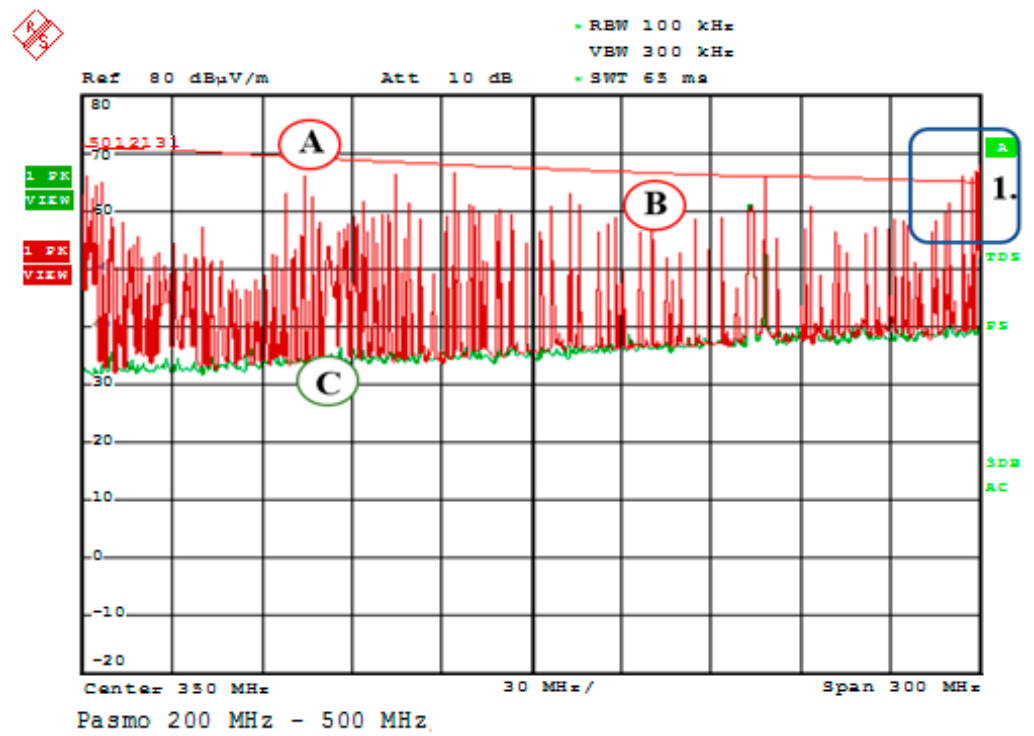


Figure 13. Spectrum of interfering signals radiated by a rail vehicle travelling at a speed of 50 km/h and the electromagnetic background for a frequency range of 200 MHz–500 MHz.

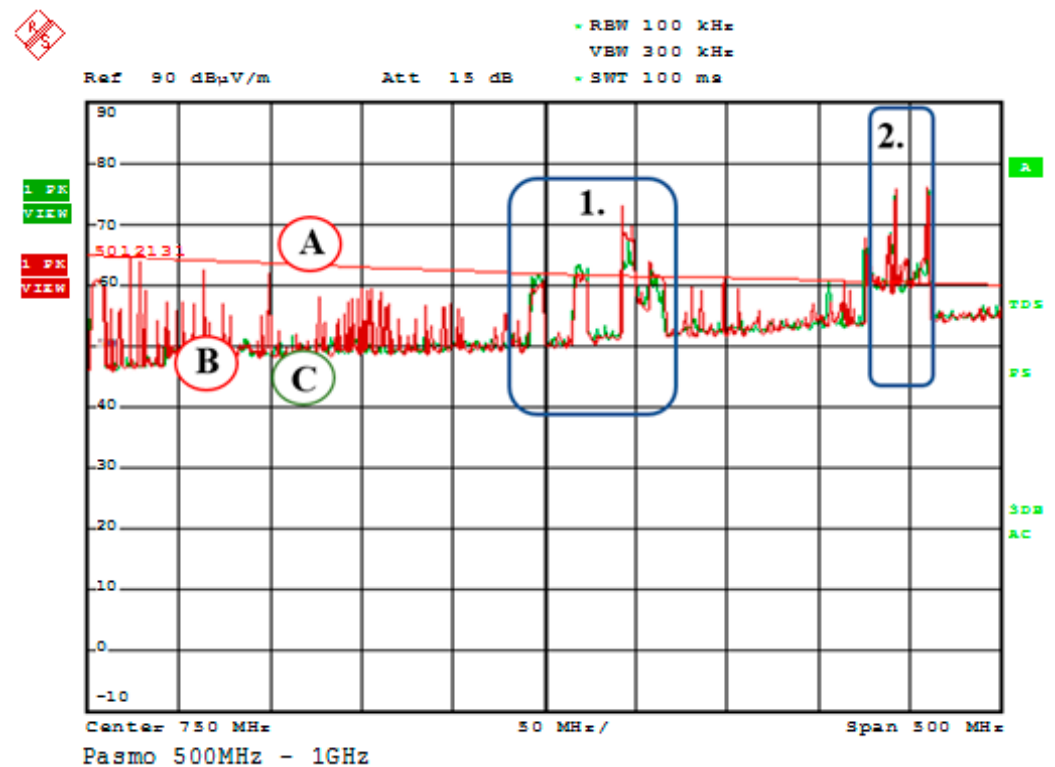


Figure 14. Spectrum of interfering signals radiated by a rail vehicle travelling at a speed of 50 km/h and the electromagnetic background for a frequency range of 500 MHz–1 GHz.

In the case of the signal spectra for a frequency range of 150 kHz–1.15 MHz, shown in Figure 9, both the interfering signals radiated by a traction vehicle travelling at a speed of 50 km/h and the electromagnetic background level do not exceed the permissible values set out in PN-EN 50121-3-1. However, please note that the level of interfering signals radiated

by a travelling rail vehicle increased significantly, which is also shown in Table 2. For example, an interfering signal level change by as much as 44.6 dB $\mu$ A/m has been observed for the frequency of 0.34 MHz, which is a very high value for this measurement subrange (frequency band).

**Table 2.** Measurement method and the results obtained for individual frequency ranges for a rail vehicle travelling at a speed of 50 km/h and the OETD electromagnetic background level.

No.	Detector	Frequency [MHz]	Level Background [dB $\mu$ A/m]	Level Driving 50 km/h [dB $\mu$ A/m]
1	Peak	0.34	−1.1	43.5
2	Peak	0.59	−0.5	39.1
3	Peak	0.79	0.4	28.2
4	Peak	0.91	2.5	25.5
5	Peak	1.21	−10	8.7

In the case of the signal spectra for a frequency range of 1 MHz–11 MHz, shown in Figure 10, the radiated interfering signals of both the electromagnetic background (marked as C) and a rail vehicle travelling at a speed of 50 km/h (marked as B) do not exceed the permissible values set out in PN-EN 50121-3-1. However, please note the clustering of individual spectral lines around selected frequencies marked in Figure 10 as 1, 2, 3, and 4. These frequencies are characteristic of a rail vehicle onboard equipment and result from these signals processed within a locomotive. However, please note that the level of interfering signals radiated by a travelling rail vehicle increased significantly, as shown in Table 3. The interfering signal level change to as much as 41.3 dB $\mu$ A/m has been observed for the frequency of 1.76 MHz. This is a very high value for this measurement subrange, resulting from operating a rail vehicle on a track.

**Table 3.** Measurement method and the results obtained for individual frequency ranges for a rail vehicle travelling at a speed of 50 km/h, and the OETD electromagnetic background level.

No.	Detector	Frequency [MHz]	Level Background [dB $\mu$ A/m]	Level Driving 50 km/h [dB $\mu$ A/m]
1	Peak	1.76	−12.1	29.2
2	Peak	2.85	12.2	23.6
3	Peak	4.25	1.8	29.8
4	Peak	7.62	−2.2	6.2
5	Peak	10.01	−12.2	−2.1

Table 3 shows measurement results for a travelling vehicle and the electromagnetic background level for a signal spectrum, where the electromagnetic field strength increase is the highest.

The signal spectra for a frequency range of 10 MHz–30 MHz shown in Figure 9 indicate that the interfering signals radiated by a traction vehicle travelling at a speed of 50 km/h (marked as B) exceed the permissible values set out in PN-EN 50121-3-1. This exceedance is evident for a frequency range of 27.09 MHz and results from the operation of an ETCS transmitter (vehicle antenna, European Train Control System track)—marked in Figure 11 as 1. Please note the clustering of individual spectral lines around the frequencies that are characteristic of a travelling vehicle. It can be observed that the interfering signal level of a travelling rail vehicle increased only slightly (relative to background measurement), e.g., an interfering signal change to 38.4 dB $\mu$ A/m was observed for a frequency of 27.09 MHz. Table 4 shows the background and travelling vehicle measurements for a signal spectrum, where the electromagnetic field strength increase is the highest.

**Table 4.** Measurement method and results obtained for individual frequencies, for a rail vehicle travelling at a speed of 50 km/h and the electromagnetic background.

No.	Detector	Frequency [MHz]	Level Background [dB $\mu$ A/m]	Level Driving 50 km/h [dB $\mu$ A/m]
1	Peak	12.96	20.1	22.1
2	Peak	13.24	10	16.8
3	Peak	13.88	8.2	20.0
4	Peak	15.74	9.9	12.8
5	Peak	17.85	−8.9	4.9
6	Peak	19.84	−10.6	−0.11
7	Peak	22.18	−10.4	−0.11
8	Peak	27.09 <sup>1</sup> ETCS	−11.9	26.5

<sup>1</sup> ETCS—Vehicle-track antenna of the European Train Control System.

The spectra for a frequency range of 30 MHz–230 MHz shown in Figure 12 clearly indicate that the interfering signals radiated by a traction vehicle travelling at a speed of 50 km/h (marked as B) exceed the permissible values set out for various subranges in PN-EN 50121-3-1, which is marked in the Figure as 1 and 4. This exceedance is particularly evident for the frequencies of 161.4 and 204.3 MHz. Please note the appearance of spectral lines (parasitic signals) at other frequencies. Their values are significant for a travelling vehicle. The interfering signal level during the travel of a rail vehicle increased considerably, which can be observed in Figure 12 and is additionally shown in Table 5. The graph illustrating the signal spectrum electromagnetic background measurement does not contain specific interfering signals. However, they appear during movement, which can be interpreted as the appearance of harmonic signals in the power supply and processing lines of the onboard locomotive equipment (installed), e.g., traction converters, inverters, and switches, when increasing the grid power demand.

**Table 5.** Measurement method and results were obtained for individual frequencies, for a rail vehicle travelling at a speed of 50 km/h and the electromagnetic background.

No.	Detector	Frequency [MHz]	Level Background [dB $\mu$ A/m]	Level Driving 50 km/h [dB $\mu$ A/m]
1	Peak	41.5	40	73.8
2	Peak	79.5	34.5	76.2
3	Peak	101.2	48.8	72.3
4	Peak	154.5	41.8	74.2
5	Peak	161.4	42.1	75.1
6	Peak	204.3	43.6	71.8

The spectra for the frequency range of 200 MHz–500 MHz in Figure 13 clearly show changes in the values of radiated interfering signals for a traction unit moving at a speed of 50 km/h (marked as B). However, the permissible value specified in the standard is shown to be exceeded only at the end of the analysed spectrum analyser band, which is marked in Figure 1 as 1. Exceeding this value is particularly evident at a frequency of 495.88 MHz (Table 6).

**Table 6.** Measurement method and results were obtained for individual frequencies, for a rail vehicle travelling at a speed of 50 km/h and the electromagnetic background.

No.	Detector	Frequency [MHz]	Level Background [dB $\mu$ A/m]	Level Driving 50 km/h [dB $\mu$ A/m]
1	Peak	200.03	32.1	66.4
2	Peak	274.85	33.6	66.9
3	Peak	309.95	33.8	67.3
4	Peak	325.52	34.1	67.6
5	Peak	427.65	52.2	66.9
6	Peak	495.88	39.8	67.9

The interfering signal spectrum also contains other parasitic signal lines of values significant to a moving vehicle (not present when measuring the electromagnetic background). The levels of interfering signals with such amplitudes and simultaneously within the high-frequency range may adversely impact the operation of, e.g., VMS cameras, where the video, control and power signals are routed through power cables over very long distances or transmitted as wireless. For this frequency range, the radiated interfering signal may induce undesired voltage or distort the video signal inside such a device, in the case of incorrect connection, discontinuity in ensuring screening, and also through the process openings of the camera (e.g., introduced elements for image adjustment at the camera installation location).

Figure 14 shows the spectra for a frequency range of 500 MHz–1 GHz. The presented waveforms clearly show they exceeded permissible interfering signal values for two rail vehicle test modes—background and movement. This exceedance is evident, particularly for two frequency subranges, marked in Figure 14 as 1 and 2. At the same time, the interfering signal band is much wider for signals clustered around frequencies above 500 MHz (Table 7). The levels of interfering signals with such amplitudes and very high frequencies may distort the correct operation of a VMS. For this frequency range, an incorrect connection, no screening or a video, control or power cable improperly terminated and connected with the ground may constitute an interfering signal receiving antenna.

**Table 7.** Measurement method and results obtained for individual frequencies, for a rail vehicle travelling at a speed of 50 km/h and the electromagnetic background.

No.	Detector	Frequency [MHz]	Level Background [dB $\mu$ A/m]	Level Driving 50 km/h [dB $\mu$ A/m]
1	Peak	523.2	48.1	54.9
2	Peak	525.8	48.2	54.2
3	Peak	599.5	49.1	61.8
4	Peak	749.6	60.1	60.2
5	Peak	881.2	62.2	72.4
6	Peak	947.3	75.1	75.9
7	Peak	962.4	75.9	76.1

In addition, production (process) openings located on metal housings of VMS devices constitute slot antennas that enable undesirable interfering signals to penetrate inside the housing. This leads to the possible induction of voltages from these frequency ranges on the outside of these devices, which has an adverse effect on the functioning of all security systems operated within an extensive railway area, the tested VMS in this case.

Rail vehicles moving with a speed greater than 50 km/h will generate higher interference spectrum signal amplitudes within this frequency range. This is related to the higher consumption of the current from the railway overhead contact line. The power of the consumers installed onboard a rail vehicle will be burdened with the higher currents associated with increased speed, particularly in the case of power and electronic devices such as voltage transformers in a locomotive or traction motors. The authors intend to

implement such research in the future to be able to demonstrate the impact of vehicles moving during such tests at speeds different than 50 km/h. This will be a study of an experimental nature, deviating from the requirements of the standard.

3.2. The Impact of Radiated Interference Generated by a Rail Vehicle on the Operation of Selected VMS Elements

An external electromagnetic field radiated by a rail vehicle in the high-frequency range penetrates inside security system VMS camera circuits through the mechanisms of direct electromagnetic field coupling, inducing fault current  $I_i$  in the power, signal, video and control cables. Due to the impedance  $Z_k$  of the aforementioned cables, the flowing fault current induces voltage  $U_i$ , which may impact the camera’s electronic output elements, e.g., the output amplifier operating point, as shown in Figure 15. Through these cables, the video signal transmission bus and the power and control cables for a VMS device, e.g., a camera, “collect” the high-frequency fault current generated unintentionally by a rail vehicle travelling at a speed of 50 km/h. In particular, this effect occurs for a frequency range above 200 MHz, which is also evident in Figure 14, showing the interfering signal spectrum for a frequency band of 500 MHz–1 GHz. Incorrect cables routed to the cameras can constitute receiving antennas in the case of these interfering signal frequencies. Particularly in the event of unprofessional termination—connection of the screen to the ground (camera metal housing). In addition, the process of “openings and slots” of a camera employed to introduce/route out cables and local camera technical parameter adjustment may become slot antennas that receive interference signals from a rail vehicle, as shown in Figure 1. Impacted by an undesirable electromagnetic field, the fault current induced in the a/m cables and electronic output elements of a camera may, e.g., change the operating point of active output amplifier elements, leading to signal distortions. The useful signal, together with the fault current, also leads to a change in the reference potential of the camera as a result of coupling through mutual impedance  $Z_k$ .

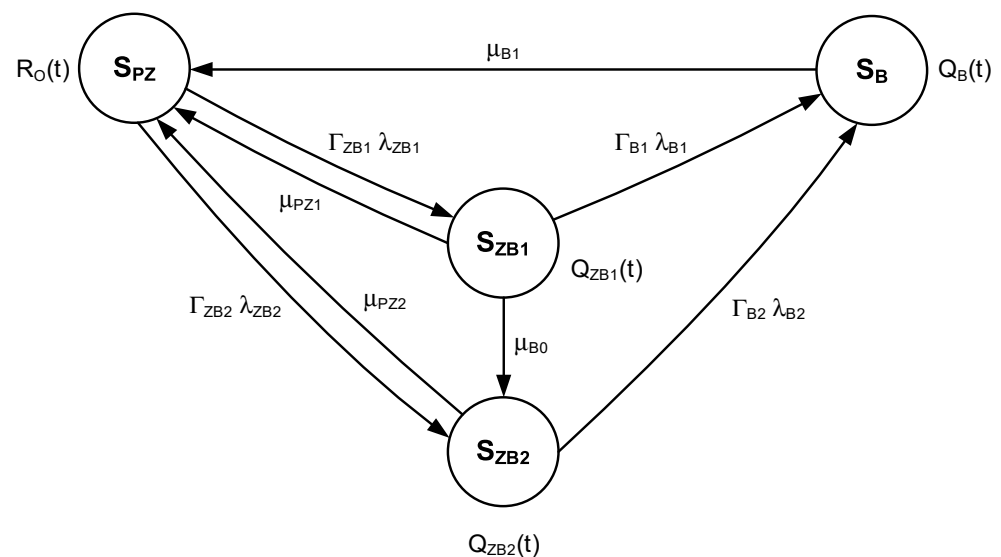


Figure 15. A graph illustrating the impact of emitted radiated interference generated by a rail traction vehicle on a trackside video monitoring system.

A camera placed in a tamper-proof metal housing executes two coupling types—direct serial coupling by the radiated interfering electromagnetic field originating from the rail vehicle and parallel coupling by passive elements,  $Z_k$  and  $C_{p1}$ ,  $C_{p1}$  (cable—metal housing parasitic capacitances) in this case. The coupling is also implemented by parasitic capacitance  $C_{pp}$  of the camera electronic output board—PCB, relative to the VMS camera metal housing. Parasitic coupling between the PCB and the VMS camera metal housing can be minimized by reducing the parasitic capacitance  $C_{pp}$  between a circuit particularly

sensitive to camera distortions and the ground or by reducing rapid voltage changes ( $dU_i/dt$ ), which occur within a passive element and are beyond our control since they are generated by a rail vehicle.

In addition, the occurrence of  $U_i$  interference on the  $Z_k$  impedance creates a possibility of an additional coupling through the so-called crosstalk of inductive or capacitive nature. It occurs within long cables between the VMS camera and the alarm receiving centre. In such a case, the difference in the potential (interference voltage  $U_i$ ) between the cable (signal, control or power) and the metal camera housing always generates an alternating electric field around this conductor.

The electromagnetic field change generates current as it occurs, which is induced in the aforementioned cables in the case of no screening, damage or discontinuity. These cables are always near a bus for transmitting a video signal from a railway area. In such a case, we are dealing with the so-called capacitive crosstalk (cameras are also powered through signal cables or POE). Capacitive crosstalk coupling is always implemented by interfering signals. The crosstalk occurring within a camera output circuit ( $r$ ) is always proportional to the rate of changes in this interfering voltage over time, as shown in Figure 15. In the event of inductive crosstalk for previously discussed cases, particularly important is the rate of current changes over time ( $dI_i/dt$ ), which may be generated within cables due to inductance or demand changes, e.g., in the overhead contact line or power line supplying an entire extensive railway area.

#### 4. Assessment of the Impact of Emitted Radiated Interference Generated by a Rail Traction Vehicle on Trackside Video Monitoring Systems

Analysing the impact of emitted radiated interference generated by a rail traction vehicle on a trackside video monitoring system makes it possible to illustrate the reliability and operational relationships, such as the example shown in Figure 15.

Designations in Figure 15:

- $R_O(t)$ —probability function of a trackside video monitoring system staying in a state of full fitness  $S_{PZ}$ ,
- $Q_{ZB1}(t)$ —probability function of a trackside video monitoring system staying in a state of partial fitness I  $S_{ZB1}$ ,
- $Q_{ZB2}(t)$ —probability function of a trackside video monitoring system staying in a state of partial fitness II  $S_{ZB2}$ ,
- $Q_B(t)$ —probability function of a trackside video monitoring system staying in a state of unfitness  $S_B$ ,
- $\lambda_{ZB1}$ —intensities of transition from a state of full fitness  $S_{PZ}$  to a state of partial fitness I  $S_{ZB1}$ ,
- $\lambda_{ZB2}$ —intensities of transition from a state of full fitness  $S_{PZ}$  to a state of partial fitness II  $S_{ZB2}$ ,
- $\mu_{PZ1}$ —intensities of transition from a state of partial fitness I  $S_{ZB1}$  to a state of full fitness  $S_{PZ}$ ,
- $\mu_{PZ2}$ —intensities of transition from a state of partial fitness II  $S_{ZB2}$  to a state of full fitness  $S_{PZ}$ ,
- $\mu_{B0}$ —intensities of transition from a state of partial fitness I  $S_{ZB1}$  to a state of full fitness II  $S_{PZ}$ ,
- $\mu_{B1}$ —intensities of transition from a state of unfitness  $S_B$  to a state of full fitness  $S_{PZ}$ ,
- $\lambda_{B1}$ —intensities of transition from a state of partial fitness I  $S_{ZB1}$  to a state of unfitness  $S_B$ ,
- $\lambda_{B2}$ —intensities of transition from a state of partial fitness II  $S_{ZB2}$  to a state of unfitness  $S_B$ ,
- $\Gamma_{ZB1}, \Gamma_{ZB2}, \Gamma_{B1}, \Gamma_{B2}$ —impact coefficients of radiated interference.

Full fitness  $S_{PZ}$  is a state in which a trackside video monitoring system functions correctly. Partial fitness  $S_{ZB1}$  is a state in which a trackside video monitoring system is partially fit (parallel coupling occurs). Partial fitness  $S_{ZB2}$  is a state in which a trackside video monitoring system is partially fit (serial coupling occurs). Unfitness  $S_B$  is a

state in which a trackside video monitoring system is unfit (radiated interference exceeds permissible values).

Suppose a trackside video monitoring system is in a state of full fitness  $S_{PZ}$  and the interference occurs in the form of parallel coupling. In that case, the system switches to a state of partial fitness I  $S_{ZB1}$  with the intensity of  $\lambda_{ZB1}$ . If a trackside video monitoring system is in a state of partial fitness I  $S_{ZB1}$ , then it is possible to switch to a state of full fitness  $S_{PZ}$ , provided that actions are taken to restore the state of fitness.

In the event of a state of partial fitness I  $S_{ZB1}$  and the interference exceeding permissible values, the system switches to a state of unfitness  $S_B$  with the intensity of  $\lambda_{B1}$ .

If a trackside video monitoring system is in a state of full fitness  $S_{PZ}$  and interference occurs in the form of parallel coupling, then the system switches to a state of partial fitness II  $S_{ZB2}$  with the intensity of  $\lambda_{ZB2}$ . Suppose a trackside video monitoring system is in a state of partial fitness II  $S_{ZB2}$ . In that case, it is possible to switch to the state of full fitness  $S_{PZ}$ , provided that actions aimed at restoring the state of fitness are taken.

In the event of a state of partial fitness II  $S_{ZB2}$  and the radiated interference exceeding permissible values, the system moves to a state of unfitness  $S_B$  with an intensity of  $\lambda_{B2}$ .

If a trackside video monitoring system is in a state of partial fitness I  $S_{ZB1}$  and radiated interference changes from parallel to serial coupling, then the system switches to a state of partial fitness II  $S_{ZB2}$  with the intensity of  $\mu_{B0}$ .

Suppose a trackside video monitoring system is in a state of unfitness  $S_B$  and remedial actions are taken to restore a state of fitness. In that case, it switches to a state of full fitness  $S_{PZ}$  with the intensity of  $\mu_{B1}$ .

The system shown in Figure 15 has been characterized by the following Chapman–Kolmogorov equations:

$$\begin{aligned}
 R'_0(t) &= -\Gamma_{ZB1} \cdot \lambda_{ZB1} \cdot R_0(t) + \mu_{PZ1} \cdot Q_{ZB1}(t) - \Gamma_{ZB2} \cdot \lambda_{ZB2} \cdot R_0(t) + \mu_{PZ2} \cdot Q_{ZB2}(t) + \mu_{B1} \cdot Q_B(t) \\
 Q'_{ZB1}(t) &= \Gamma_{ZB1} \cdot \lambda_{ZB1} \cdot R_0(t) - \mu_{PZ1} \cdot Q_{ZB1}(t) - \Gamma_{B1} \cdot \lambda_{B1} \cdot Q_{ZB1}(t) - \mu_{B0} \cdot Q_{ZB1}(t) \\
 Q'_{ZB2}(t) &= \Gamma_{ZB2} \cdot \lambda_{ZB2} \cdot R_0(t) - \mu_{PZ2} \cdot Q_{ZB2}(t) - \Gamma_{B2} \cdot \lambda_{B2} \cdot Q_{ZB2}(t) + \mu_{B0} \cdot Q_{ZB1}(t) \\
 Q'_B(t) &= \Gamma_{B1} \cdot \lambda_{B1} \cdot Q_{ZB1}(t) + \Gamma_{B2} \cdot \lambda_{B2} \cdot Q_{ZB2}(t) - \mu_{B1} \cdot Q_B(t)
 \end{aligned}
 \tag{1}$$

By adopting the following initial conditions:

$$\begin{aligned}
 R_0(0) &= 1 \\
 Q_{ZB1}(0) &= Q_{ZB2}(0) = Q_B(0) = 0
 \end{aligned}
 \tag{2}$$

and using mathematical transformations (including the Laplace transform), the sought-after probability of a trackside video monitoring system staying in a state of full fitness was calculated for the following input data:

- Research duration—1 year (this time is given in hours [h]):

$$t = 8760[h]$$

- Intensities of transitions from a state of full fitness to a state of partial fitness I  $\lambda_{ZB1}$ :

$$\lambda_{ZB1} = 0.000001$$

- Intensity of transitions from a state of full fitness to a state of partial fitness II  $\lambda_{ZB2}$ :

$$\lambda_{ZB2} = 0.0000001$$

- Intensity of transitions from a state of partial fitness I to a state of unfitness  $\lambda_{B1}$ :

$$\lambda_{B1} = 0.0000001$$

- Intensity of transitions from a state of partial fitness II to a state of unfitness  $\lambda_{B2}$ :

$$\lambda_{B2} = 0.000001$$

- Intensity of transitions from a state of partial fitness I to a state of full fitness II  $\mu_{B0}$ :

$$\mu_{B0} = 0.00000001$$

- Intensity of transitions from a state of unfitness to a state of full fitness  $\mu_{B1}$ :

$$\mu_{B1} = 0.01$$

- Intensity of transitions from a state of partial fitness I to a state of full fitness  $\mu_{PZ1}$ :

$$\mu_{PZ1} = 0.1$$

- Intensity of transitions from a state of partial fitness II to a state of full fitness  $\mu_{PZ2}$ :

$$\mu_{PZ2} = 0.2$$

- Radiated interference impact coefficients:

$$\Gamma_{ZB1} = \Gamma_{ZB2} = \Gamma_{B1} = \Gamma_{B2} = 0.5$$

As a result of the adopted input data, using the system of Equations (1), we get:

$$R_0^*(s) = \frac{1.080004 \cdot 10^{14} \cdot s + 10^{14} \cdot \mu_{PZ1} + 8 \cdot 10^{12} \cdot \mu_{PZ2} + 2 \cdot 10^{22} \cdot s^2 \cdot \mu_{PZ1} + 2 \cdot 10^{22} \cdot s^2 \cdot \mu_{PZ2} + 2.000108 \cdot 10^{20} \cdot s^2 + 2 \cdot 10^{22} \cdot s^3 + 2.0001 \cdot 10^{20} \cdot s \cdot \mu_{PZ1} + 2.000008 \cdot 10^{20} \cdot s \cdot \mu_{PZ2} + 2 \cdot 10^{20} \cdot \mu_{PZ1} \cdot \mu_{PZ2} + 2 \cdot 10^{22} \cdot s \cdot \mu_{PZ1} \cdot \mu_{PZ2} + 4 \cdot 10^6}{5.340022 \cdot 10^7 \cdot s - 2 \cdot 10^6 \cdot \mu_{PZ2} + 2.00011 \cdot 10^{20} \cdot s^2 \cdot \mu_{PZ1} + 2.000108 \cdot 10^{20} \cdot s^2 \cdot \mu_{PZ2} + 2 \cdot 10^{22} \cdot s^3 \cdot \mu_{PZ1} + 2 \cdot 10^{22} \cdot s^3 \cdot \mu_{PZ2} + 2.1800634 \cdot 10^{14} \cdot s^2 + 2.000218 \cdot 10^{20} \cdot s^3 + 2 \cdot 10^{22} \cdot s^4 + 1.100005 \cdot 10^{14} \cdot s \cdot \mu_{PZ1} + 1.080003 \cdot 10^{14} \cdot s \cdot \mu_{PZ2} + 2 \cdot 10^{20} \cdot s \cdot \mu_{PZ1} \cdot \mu_{PZ2} + 2 \cdot 10^{22} \cdot s^2 \cdot \mu_{PZ1} \cdot \mu_{PZ2} - 1} \tag{3}$$

Ultimately, we get the relationship:

$$R_0(t) = 4.09351637 \cdot 10^{-11} \cdot e^{-0.01 \cdot t} + 2.50000904 \cdot 10^{-7} \cdot e^{-0.20000055 \cdot t} + 0.00000499 \cdot e^{-0.10000053 \cdot t} + 0.99999474 \cdot e^{9.99994349 \cdot 10^{-14} \cdot t} \tag{4}$$

and the final result:

$$R_0 = 0.99999475 \tag{5}$$

The impact of EMI on VMS depends on applied solutions (structural, organizational) aimed at minimizing the effect EMI has on the system’s operation. The graph presented in the article, which depicts the impact of emitting radiated interference generated by a rail traction unit on a trackside visual monitoring system and the obtained mathematical relationships, enables a numerical assessment of the applied solutions aimed at mitigating the impact of EMI on VMS. In practice, this allows for the rational selection of solutions that will be effective and economically justified [91,92].

### 5. Conclusions

The research conducted by the authors indicates the significance of the issue of assessing the impact of emitted radiated interference generated by a rail traction vehicle on the operational process of trackside video monitoring systems. Despite the application of numerous solutions (whether structural or organizational), permissible values specified in relevant standards are still exceeded. Such events may lead to incorrect functioning of the devices used within the rail transport process. Actual tests conducted on a test Track at the Railway Institute confirmed the occurrence of such situations. This is why the next stage of the authors’ research was to develop a graph illustrating the impact of emitted radiated interference generated by a rail traction vehicle on a trackside video monitoring system (taking into account the impact coefficients of radiated interference).

The conducted mathematical calculations enabled obtaining a relationship to calculate the probability of trackside video monitoring systems remaining in a state of full fitness. A practical application of the obtained relationships allows determining the impact of applied solutions reducing the impact of interference radiated by a rail traction vehicle on the operational process of trackside video monitoring systems. In practice, this enables the rational selection of solutions that are efficient and economically viable in terms of deployment at the same time.

Further research by the authors will be aimed at conducting successive measurements at the test track at the Railway Institute, using a different rolling stock type. The second direction of the authors' research targets developing structural solutions to improving the resistance of trackside video monitoring systems to radiated interference.

**Author Contributions:** Conceptualization, J.P., A.R., and M.S; methodology, A.R., J.P., and P.W.; validation, J.P., A.R., and K.B.; formal analysis, J.P., A.R., T.K., and M.S; investigation, J.P., T.K., A.R., and P.W.; resources, J.P., and A.R.; data curation, A.R., J.P., P.W., and K.B.; writing—original draft preparation, J.P., A.R., and P.W.; writing—review and editing, J.P., A.R., K.B., P.W., T.K., and M.S.; visualization, J.P., and A.R.; supervision, J.P., and A.R.; project administration, J.P., and A.R. All authors have read and agreed to the published version of the manuscript.

**Funding:** This work was co-financed by the Military University of Technology under research project UGB 737. This paper was co-financed by a research grant from the Warsaw University of Technology supporting scientific activity in the discipline of civil engineering and transport.

**Data Availability Statement:** The data presented in this study are available on request from the corresponding author.

**Conflicts of Interest:** The authors declare no conflict of interest.

## Abbreviations

### List of Important Abbreviations and Symbols.

No.	Full Name for Abbreviation	Abbr.
1	Alarm Receiving Centre	ARC
2	Electronic Security Systems	ESS
3	European Train Control System	ETCS
4	Global System for Mobile Communications	GSM
5	GSM for Railways	GSM-R
6	State Critical Infrastructure	SCI
7	Intensities of damage	$\lambda$
8	Intensities of repairs	$\mu$
9	Railway Institute Test Track Operation Centre	OETD
10	State Fire Service	PSP
11	State of Partial Fitness	$S_{ZB}$
12	State of Full Fitness	$S_{PZ}$
13	State of Unfitness	$S_B$
14	Video Monitoring System	VMS
15	Fire Alarm System	FAS

## References

1. Arriaga, J.; Medellin, G.; Ojeda, E.; Salles, P. Shoreline Detection Accuracy from Video Monitoring Systems. *J. Mar. Sci. Eng.* **2022**, *10*, 95. [\[CrossRef\]](#)
2. Brignone, M.; Schiaffino, C.; Isla, F.; Ferrari, M. A system for beach video-monitoring: Beachkeeper plus. *Comput. Geosci.* **2012**, *49*, 53–61. [\[CrossRef\]](#)
3. Van Enckevort, I.; Ruessink, B. Video observations of nearshore bar behaviour. Part 2: Alongshore non-uniform variability. *Cont. Shelf Res.* **2003**, *23*, 513–532. [\[CrossRef\]](#)
4. Siergiejczyk, M.; Kasprzyk, Z.; Rychlicki, M.; Szmigiel, P. Analysis and Assessment of Railway CCTV System Operating Reliability. *Energies* **2022**, *15*, 1701. [\[CrossRef\]](#)
5. Pastuszek, G.; Jakubowski, M. Adaptive computationally scalable motion estimation for the hardware H.264/AVC encoder. *IEEE Trans. Circuits Syst. Video Technol.* **2013**, *23*, 802–812. [\[CrossRef\]](#)
6. Gang, H.; Ma, X.; Liu, L. Design of unattended facilities of remote wireless monitoring system. *Appl. Sci. Technol.* **2007**, *34*, 58.
7. Zhen, S.; Qingdang, L.; Lu, W.; Junfei, W. A Distributed Video Monitoring System Architecture for Semantic Retrieval. In Proceedings of the 2019 2nd International Conference on Safety Produce Informatization (IICSPI), Chongqing, China, 28–30 November 2019; pp. 574–577. [\[CrossRef\]](#)
8. Zheng, D.; Wang, Y.; Li, H.; Wu, H.; Yuan, G. Research on Wireless Video Monitoring System Based on Hisilicon Platform. In *Advances in Natural Computation, Fuzzy Systems and Knowledge Discovery; ICNC-FSKD 2020. Lecture Notes on Data Engineering and Communications Technologies*; Meng, H., Lei, T., Li, M., Li, K., Xiong, N., Wang, L., Eds.; Springer: Cham, Switzerland, 2021; Volume 88. [\[CrossRef\]](#)
9. Wu, H.; Xu, D.; Yuan, G. Region covariance based total variation optimization for structure-texture decomposition. *Multimed. Tools Appl.* **2018**, *77*, 16985–17005. [\[CrossRef\]](#)
10. Klimczak, T.; Paś, J. *Basics of Exploitation of Fire Alarm Systems in Transport Facilities*; Military University of Technology: Warsaw, Poland, 2020.
11. Jakubowski, K.; Paś, J.; Duer, S.; Bugaj, J. Operational Analysis of Fire Alarm Systems with a Focused, Dispersed and Mixed Structure in Critical Infrastructure Buildings. *Energies* **2021**, *14*, 7893. [\[CrossRef\]](#)
12. Rosiński, A. *Modelling the Maintenance Process of Transport Telematics Systems*; Publishing House Warsaw University of Technology: Warsaw, Poland, 2015.
13. Jakubowski, K.; Paś, J.; Rosiński, A. The Issue of Operating Security Systems in Terms of the Impact of Electromagnetic Interference Generated Unintentionally. *Energies* **2021**, *14*, 8591. [\[CrossRef\]](#)
14. Dziula, P.; Paś, J. Low Frequency Electromagnetic Interferences Impact on Transport Security Systems Used in Wide Transport Areas. *TransNav Int. J. Mar. Navig. Saf. Sea Transp.* **2018**, *12*, 251–258. [\[CrossRef\]](#)
15. Siergiejczyk, M.; Paś, J.; Dudek, E. Reliability analysis of aerodrome's electronic security systems taking into account electromagnetic interferences. In *Safety and Reliability-Theory and Applications, Proceedings of the 27th European Safety and Reliability Conference (Esrel 2017), Portorož, Slovenia, 18–22 June 2017*; Cepin, M., Briš, R., Eds.; CRC Press/Balkema: Schipholewh, The Netherlands, 2017; pp. 2285–2292.
16. Krzykowski, M.; Paś, J.; Rosiński, A. Assessment of the level of reliability of power supplies of the objects of critical infrastructure. *IOP Conf. Ser. Earth Environ. Sci.* **2019**, *214*, 012018. [\[CrossRef\]](#)
17. Paś, J.; Klimczak, T.; Rosiński, A.; Stawowy, M. The Analysis of the Operational Process of a Complex Fire Alarm System Used in Transport Facilities. *Build. Simul.* **2022**, *15*, 615–629. [\[CrossRef\]](#)
18. Stawowy, M.; Olchowik, W.; Rosiński, A.; Dąbrowski, T. The Analysis and Modelling of the Quality of Information Acquired from Weather Station Sensors. *Remote Sens.* **2021**, *13*, 693. [\[CrossRef\]](#)
19. Zieja, M.; Szelmanowski, A.; Pazur, A.; Kowalczyk, G. Computer Life-Cycle Management System for Avionics Software as a Tool for Supporting the Sustainable Development of Air Transport. *Sustainability* **2021**, *13*, 1547. [\[CrossRef\]](#)
20. Kossakowski, D.; Krzykowska, K. Application of V2X Technology in Communication between Vehicles and Infrastructure in Chosen Area. In *Research Methods and Solutions to Current Transport Problems, Proceedings of the International Scientific Conference Transport of the 21st Century, Advances in Intelligent Systems and Computing, Ryn, Poland, 9–12 June 2019*; Siergiejczyk, M., Krzykowska, K., Eds.; Springer: Cham, Switzerland, 2020; Volume 1032, pp. 247–256.
21. Suproniuk, M.; Paś, J. Analysis of electrical energy consumption in a public utility buildings. *Przegląd Elektrotechniczny* **2019**, *95*, 97–100. [\[CrossRef\]](#)
22. Kołowrocki, K.; Soszyńska-Budny, J. Critical Infrastructure Safety Indicators. In Proceedings of the 2018 IEEE International Conference on Industrial Engineering and Engineering Management (IEEM), Bangkok, Thailand, 16–19 December 2018; pp. 1761–1764. [\[CrossRef\]](#)
23. Duer, S.; Scaticailov, S.; Paś, J.; Duer, R.; Bernatowicz, D. Taking decisions in the diagnostic intelligent systems on the basis information from an artificial neural network. *MATEC Web Conf.* **2018**, *178*, 07003. [\[CrossRef\]](#)
24. Selech, J.; Andrzejczak, K. An aggregate criterion for selecting a distribution for times to failure of components of rail vehicles. *Ekspluat. I Niezawodn.* **2020**, *22*, 102–111. [\[CrossRef\]](#)
25. Dyduch, J.; Paś, J.; Rosiński, A. *The Basic of the Operation of Transport Electronic Systems*; Publishing House of Radom University of Technology: Radom, Poland, 2011.

26. Siergiejczyk, M.; Stawowy, M. Modelling of uncertainty for continuity quality of Power supply. In *Risk, Reliability, and Safety: Innovating Theory and Practice: Modelling of Uncertainty for Continuity Quality of Power Supply, Proceedings of the ESREL2016, Glasgow, Scotland, 25–29 September 2016*; Walls, L., Revie, M., Bedford, T., Eds.; CRC Press/Balkema: London, UK, 2017; pp. 667–671.
27. Holtz, J.; Keliń, H.-J. The propagation of harmonic currents generated by inverter-fed locomotives in the distributed overhead supply system. *IEEE Trans. Power Electron.* **1989**, *4*, 168–174. [[CrossRef](#)]
28. Liu, Q.; Wu, M.; Li, J.; Yang, S. Frequency-Scanning Harmonic Generator for (Inter)Harmonic Impedance Tests and Its Implementation in Actual  $2 \times 25$  kV Railway Systems. *IEEE Trans. Ind. Electron.* **2021**, *68*, 4801–4811. [[CrossRef](#)]
29. Mollerstedt, E.; Bernhardsson, B. Out of control because of harmonics—an analysis of the harmonic response of an inverter locomotive. *IEEE Control. Syst. Mag.* **2000**, *20*, 70–81. [[CrossRef](#)]
30. Liu, Z.; Zhang, G.; Liao, Y. Stability Research of High-Speed Railway EMUs and Traction Network Cascade System Considering Impedance Matching. *IEEE Trans. Ind. Appl.* **2016**, *52*, 4315–4326. [[CrossRef](#)]
31. Semlyen, A.; Eggleston, J.F.; Arrillaga, J. Admittance Matrix Model of a Synchronous Machine for Harmonic Analysis. *IEEE Trans. Power Syst.* **1987**, *2*, 833–839. [[CrossRef](#)]
32. Paś, J.; Rosiński, A.; Chrzan, M.; Białek, K. Reliability-Operational Analysis of the LED Lighting Module Including Electromagnetic Interference. *IEEE Trans. Electromagn. Compat.* **2020**, *62*, 2747–2758. [[CrossRef](#)]
33. Siergiejczyk, M.; Rosiński, A. Analysis of power supply maintenance in transport telematics system. *Solid State Phenom.* **2014**, *210*, 14–19. [[CrossRef](#)]
34. Zhang, X.; Chen, J.; Qiu, R.; Liu, Z. VCT-AOC Comprehensive Method to Suppress High-Frequency Resonance and Low-Frequency Oscillation in Railway Traction Power Supply System. *IEEE Access* **2019**, *7*, 152202–152213. [[CrossRef](#)]
35. Wang, W.; Mingli, W.; Sun, J. Analysis of Low-Frequency Oscillation in Electric Railways Based on Small-Signal Modeling of Vehicle-Grid System in dq Frame. *IEEE Trans. Power Electron.* **2015**, *30*, 5318–5330. [[CrossRef](#)]
36. Danielsen, S.; Fosso, O.B.; Molinas, M.; Suul, J.A.; Toftevaag, T. Simplified models of a single-phase power electronic inverter for railway power system stability analysis—Development and evaluation. *Electr. Power Syst. Res.* **2010**, *80*, 204–214. [[CrossRef](#)]
37. Zhao, Y.; Ren, L.; Lin, G.; Peng, F. Research on the Harmonics Penetration Characteristics of the Traction Network to Three-Phase 380 V Power System of the Traction Substation and Suppression Scheme. *IEEE Access* **2020**, *8*, 195359–195369. [[CrossRef](#)]
38. Langella, R.; Sollazzo, A.; Testa, A. Modeling waveform distortion produced by DC locomotive conversion system. Part 2: Italian railway system. In *Proceedings of the 2004 11th International Conference on Harmonics and Quality of Power (IEEE Cat. No.04EX951)*, Lake Placid, NY, USA, 12–15 September 2004; pp. 483–488.
39. Holtz, J.; Krahn, J.O. Suppression of time-varying resonances in the power supply line of AC locomotives by inverter control. *in IEEE Trans. Ind. Electron.* **1992**, *39*, 223–229. [[CrossRef](#)]
40. Szkopiński, J.; Kochan, A. Energy Efficiency and Smooth Running of a Train on the Route While Approaching Another Train. *Energies* **2021**, *14*, 7593. [[CrossRef](#)]
41. Suarez, J.; Ladoux, P.; Roux, N.; Caron, H.; Guillaume, E. Measurement of locomotive input admittance to analyse low frequency instability on AC rail networks. In *Proceedings of the 2014 International Symposium on Power Electronics, Electrical Drives, Automation and Motion, Ischia, Italy, 18–20 June 2014*; pp. 790–795.
42. Polak, K.; Korzeb, J. Acoustic Signature and Impact of High-Speed Railway Vehicles in the Vicinity of Transport Routes. *Energies* **2022**, *15*, 3244. [[CrossRef](#)]
43. Naudé, H.; Beukes, J.; Minnaar, U. The Impact of Traction Load Harmonic Current Emissions on the Harmonic Assessment of Renewable Power Plants. In *Proceedings of the IECON 2019-45th Annual Conference of the IEEE Industrial Electronics Society, Lisbon, Portugal, 14–17 October 2019*; Volume 1, pp. 4764–4769.
44. Stackler, C.; Morel, F.; Ladoux, P.; Dworakowski, P. 25 kV–50 Hz railway supply modelling for medium frequencies (0–5 kHz). In *Proceedings of the 2016 International Conference on Electrical Systems for Aircraft, Railway, Ship Propulsion and Road Vehicles & International Transportation Electrification Conference (ESARS-ITEC)*, Toulouse, France, 2–4 November 2016; pp. 1–6.
45. Cui, H.; Feng, X.; Ge, X.; Fang, H.; Song, W. Resonant harmonic elimination pulse width modulation-based high-frequency resonance suppression of high-speed railways. *IET Power Electron.* **2015**, *8*, 735–742. [[CrossRef](#)]
46. Amin, M.; Molinas, M. Small-Signal Stability Assessment of Power Electronics Based Power Systems: A Discussion of Impedance- and Eigenvalue-Based Methods. *IEEE Trans. Ind. Appl.* **2017**, *53*, 5014–5030. [[CrossRef](#)]
47. Cao, W.; Ma, Y.; Wang, F. Sequence-impedance-based harmonic stability analysis and controller parameter design of three-phase inverter-based multibus AC power systems. *IEEE Trans. Power Electron.* **2017**, *32*, 7674–7693. [[CrossRef](#)]
48. Hu, H.; Tao, H.; Wang, X.; Blaabjerg, F.; He, Z.; Gao, S. Train-network interactions and stability evaluation in high-speed railways—Part II: Influential factors and verifications factors and verifications. *IEEE Trans. Power Electron.* **2018**, *33*, 4643–4659. [[CrossRef](#)]
49. Densem, T.J.; Bodger, P.S.; Arrillaga, J. Three Phase Transmission System Modelling for Harmonic Penetration Studies. *IEEE Trans. Power Appar. Syst.* **1984**, *PAS-103*, 310–317. [[CrossRef](#)]
50. Arrillaga, J.; Medina, A.; Lisboa, M.L.V.; Cavia, M.A.; Sanchez, P. The Harmonic Domain. A frame of reference for power system harmonic analysis. *IEEE Trans. Power Syst.* **1995**, *10*, 433–440. [[CrossRef](#)]
51. Enslin, J.H.R.; Heskes, P.J.M. Harmonic interaction between a large number of distributed power inverters and the distribution network. *IEEE Trans. Power Electron.* **2004**, *19*, 1586–1593. [[CrossRef](#)]

52. Wang, F.; Duarte, J.L.; Hendrix, M.A.M.; Ribeiro, P.F. Modeling and Analysis of Grid Harmonic Distortion Impact of Aggregated DG Inverters. *IEEE Trans. Power Electron.* **2011**, *26*, 786–797. [[CrossRef](#)]
53. Aceiton, R.; Weber, J.; Bernet, S. Input Filter for a Power Electronics Transformer in a Railway Traction Application. *IEEE Trans. Ind. Electron.* **2018**, *65*, 9449–9458. [[CrossRef](#)]
54. Song, K.; Konstantinou, G.; Mingli, W.; Acuna, P.; Aguilera, R.P.; Agelidis, V.G. Windowed SHE-PWM of Interleaved Four-Quadrant Converters for Resonance Suppression in Traction Power Supply Systems. *IEEE Trans. Power Electron.* **2017**, *32*, 7870–7881. [[CrossRef](#)]
55. Caramia, P.; Morrone, M.; Varilone, P.; Verde, P. Interaction between supply system and EMU loco in 15 kV-16/sup 2/3/ Hz AC traction systems. In Proceedings of the 2001 Power Engineering Society Summer Meeting. Conference Proceedings (Cat. No.01CH37262), Vancouver, BC, Canada, 15–19 July 2001; Volume 1, pp. 198–203.
56. Wu, L.; Mingli, W. Single-phase cascaded H-bridge multi-level active power filter based on direct current control in AC electric railway application. *IET Power Electron.* **2017**, *10*, 637–645. [[CrossRef](#)]
57. Trzmiel, G.; Jajczyk, J.; Kardas-Cinal, E.; Chamier-Gliszczyński, N.; Wozniak, W.; Lewczuk, K. The Condition of Photovoltaic Modules under Random Operation Parameters. *Energies* **2021**, *14*, 8358. [[CrossRef](#)]
58. Harnfors, L.; Bongiorno, M.; Lundberg, S. Input-Admittance Calculation and Shaping for Controlled Voltage-Source Converters. *IEEE Trans. Ind. Electron.* **2007**, *54*, 3323–3334. [[CrossRef](#)]
59. Blaabjerg, F.; Chen, Z.; Kjaer, S.B. Power electronics as efficient interface in dispersed power generation systems. *IEEE Trans. Power Electron.* **2004**, *19*, 1184–1194. [[CrossRef](#)]
60. Cespedes, M.; Sun, J. Impedance Modeling and Analysis of Grid-Connected Voltage-Source Converters. *IEEE Trans. Power Electron.* **2014**, *29*, 1254–1261. [[CrossRef](#)]
61. Li, J.; Wu, M.; Liu, Q. Measurement and simulation on low-frequency oscillation in the traction network of Xuzhou North Railway Hub. In Proceedings of the 2016 12th World Congress on Intelligent Control and Automation (WCICA), Guilin, China, 12–15 June 2016; pp. 1797–1802. [[CrossRef](#)]
62. De Castro, A.; Zumel, P.; Garcia, O.; Riesgo, T.; Uceda, J. Concurrent and simple digital controller of an AC/DC converter with power factor correction based on an FPGA. *IEEE Trans. Power Electron.* **2003**, *18*, 334–343. [[CrossRef](#)]
63. Zhang, C.; Molinas, M.; Rygg, A.; Cai, A. Impedance-based analysis of interconnected power electronics systems: Impedance network modeling and comparative studies of stability criteria. *IEEE J. Emerg. Sel. Top. Power Electron.* **2019**, *8*, 2520–2533. [[CrossRef](#)]
64. Zajkowski, K. The method of solution of equations with coefficients that contain measurement errors, using artificial neural network. *Neural Comput. Appl.* **2014**, *24*, 431–439. [[CrossRef](#)]
65. Duer, S.; Duer, R.; Mazuru, S. Determination of the expert knowledge base on the basis of a functional and diagnostic analysis of a technical object. *Nonconv. Technol. Rev.* **2016**, *20*, 23–29. Available online: <http://revtn.ro/index.php/revtn/article/view/115/76> (accessed on 10 January 2022).
66. Żyluk, A.; Kuźma, K.; Grzesik, N.; Zieja, M.; Tomaszewska, J. Fuzzy Logic in Aircraft Onboard Systems Reliability Evaluation—A New Approach. *Sensors* **2021**, *21*, 7913. [[CrossRef](#)] [[PubMed](#)]
67. Majewski, M.; Kacalak, W. Innovative Intelligent Interaction Systems of Loader Cranes and Their Human Operators. Advances in Intelligent Systems and Computing. In *Artificial Intelligence Trends in Intelligent Systems*; Springer: Cham, Switzerland, 2017; Volume 573, pp. 474–485. [[CrossRef](#)]
68. Duer, S.; Zajkowski, K.; Harničárová, M.; Charun, H.; Bernatowicz, D. Examination of Multivalent Diagnoses Developed by a Diagnostic Program with an Artificial Neural Network for Devices in the Electric Hybrid Power Supply System “House on Water”. *Energies* **2021**, *14*, 2153. [[CrossRef](#)]
69. Kierzkowski, A.; Kisiel, T. Simulation model of security control system functioning: A case study of the Wrocław Airport terminal. *J. Air Transport. Manag.* **2017**, *64*, 173–185. [[CrossRef](#)]
70. Burdzik, R.; Konieczny, Ł.; Figlus, T. Concept of on-board comfort vibration monitoring system for vehicles. In *Communications in Computer and Information Science, Activities of Transport Telematics, Proceedings of the 13th International Conference on Transport Systems Telematics, TST 2013, Katowice-Ustroń, Poland, 23–26 October 2013*; Mikulski, J., Ed.; Springer: Berlin/Heidelberg, Germany, 2013; Volume 395, pp. 418–425.
71. Stawowy, M.; Rosiński, A.; Siergiejczyk, M.; Perlicki, K. Quality and Reliability-Exploitation Modeling of Power Supply Systems. *Energies* **2021**, *14*, 2727. [[CrossRef](#)]
72. Stawowy, M.; Duer, S.; Paś, J.; Wawrzyński, W. Determining Information Quality in ICT Systems. *Energies* **2021**, *14*, 5549. [[CrossRef](#)]
73. Dudek, E.; Krzykowska-Piotrowska, K. Does Free Route Implementation Influence Air Traffic Management System? Case Study in Poland. *Sensors* **2021**, *21*, 1422. [[CrossRef](#)]
74. Stypułkowski, K.; Gołda, P.; Lewczuk, K.; Tomaszewska, J. Monitoring System for Railway Infrastructure Elements Based on Thermal Imaging Analysis. *Sensors* **2021**, *21*, 3819. [[CrossRef](#)]
75. Wawrzyński, W.; Mariusz, Z.; Żokowski, M.; Sigieli, N. Optimization of autonomous underwater vehicle mission planning process. *Bull. Pol. Acad. Sci. Techn. Sci.* **2022**, *70*, 1–8. [[CrossRef](#)]
76. Andrzejczak, K.; Bukowski, L. A method for estimating the probability distribution of the lifetime for new technical equipment based on expert judgement. *Ekspluat. I Niezawodn.* **2021**, *23*, 757–769. [[CrossRef](#)]

77. Sharma, A.; Singh, P.K.; Kumar, Y. An integrated fire detection system using IoT and image processing technique for smart cities. *Sustain. Cities Soc.* **2020**, *61*, 102332. [[CrossRef](#)]
78. Wu, H.; Wu, D.; Zhao, J. An intelligent fire detection approach through cameras based on computer vision methods. *Process Saf. Environ. Prot.* **2019**, *127*, 245–256. [[CrossRef](#)]
79. Wieczorek, A.N.; Konieczny, Ł.; Burdzik, R.; Wojnar, G.; Filipowicz, K.; Kuczaj, M. A Complex Vibration Analysis of a Drive System Equipped with an Innovative Prototype of a Flexible Torsion Clutch as an Element of Pre-Implementation Testing. *Sensors* **2022**, *22*, 2183. [[CrossRef](#)] [[PubMed](#)]
80. Duer, S. Assessment of the Operation Process of Wind Power Plant's Equipment with the Use of an Artificial Neural Network. *Energies* **2020**, *13*, 2437. [[CrossRef](#)]
81. Duer, S. Diagnostic system for the diagnosis of a reparable technical object, with the use of an artificial neural network of RBF type. *Neural Comput. Appl.* **2010**, *19*, 691–700. [[CrossRef](#)]
82. Jacyna, M.; Szczepański, E.; Izdebski, M.; Jasiński, S.; Maciejewski, M. Characteristics of event recorders in Automatic Train Control systems. *Arch. Transp.* **2018**, *46*, 61–70. [[CrossRef](#)]
83. Pyza, D.; Jachimowski, R.; Jacyna-Gołda, I.; Lewczuk, K. Performance of Equipment and Means of Internal Transport and Efficiency of Implementation of Warehouse Processes. *Procedia Eng.* **2017**, *187*, 706–711. [[CrossRef](#)]
84. Duer, S.; Duer, R. Diagnostic system with an artificial neural network which determines a diagnostic information for the servicing of a reparable technical object. *Neural Comput. Appl.* **2010**, *19*, 755–766. [[CrossRef](#)]
85. Duer, S. Diagnostic system with an artificial neural network in diagnostics of an analogue technical object. *Neural Comput. Appl.* **2010**, *19*, 55–60. [[CrossRef](#)]
86. Paś, J.; Rosiński, A.; Białek, K. A reliability-operational analysis of a track-side CCTV cabinet taking into account interference. *Bull. Pol. Acad. Sci. Tech. Sci.* **2021**, *69*, e136747. [[CrossRef](#)]
87. Paś, J.; Rosiński, A.; Białek, K. A reliability-exploitation analysis of a static converter taking into account electromagnetic interference. *Transp. Telecommun.* **2021**, *22*, 217–229. [[CrossRef](#)]
88. Białek, K.; Wetoszka, P. Analysis of Elimination of Electromagnetic Disturbances at Power Ports of Railway Equipment. In *Research Methods and Solutions to Current Transport Problems*; Sergiejczyk, M., Krzykowska, K., Eds.; Springer: Cham, Switzerland, 2020; Volume 1032. [[CrossRef](#)]
89. Białek, K.; Wetoszka, P.; Paś, J. Research results of selected equipment on electrostatic discharge—conclusions. *Przegląd Elektrotechniczny* **2019**, *11*, 124–126. [[CrossRef](#)]
90. Paś, J.; Klimczak, T. Selected issues of the reliability and operational assessment of a fire alarm system. *Ekspluat. I Niezawodn. Maint. Reliab.* **2019**, *21*, 553–561. [[CrossRef](#)]
91. Oszczypała, M.; Ziółkowski, J.; Małachowski, J. Analysis of Light Utility Vehicle Readiness in Military Transportation Systems Using Markov and Semi-Markov Processes. *Energies* **2022**, *15*, 5062. [[CrossRef](#)]
92. Oszczypała, M.; Ziółkowski, J.; Małachowski, J. Reliability Analysis of Military Vehicles Based on Censored Failures Data. *Appl. Sci.* **2022**, *12*, 2622. [[CrossRef](#)]